

# Aura OMI observations of regional SO<sub>2</sub> and NO<sub>2</sub> pollution changes from 2005 to 2015

Nickolay A. Krotkov<sup>1</sup>, Chris A. McLinden<sup>2</sup>, Can Li<sup>3,1</sup>, Lok N. Lamsal<sup>4,1</sup>, Edward A. Celarier<sup>4,1</sup>, Sergey V. Marchenko<sup>5,1</sup>, William H. Swartz<sup>6,1</sup>, Eric J. Bucsela<sup>7</sup>, Joanna Joiner<sup>1</sup>, Bryan N. Duncan<sup>1</sup>, K. Folkert Boersma<sup>8,9,10</sup>, J. Pepijn Veefkind<sup>9,11</sup>, Pieter F. Levelt<sup>9,11</sup>, Vitali E. Fioletov<sup>2</sup>, Russel R. Dickerson<sup>12</sup>, Hao He<sup>12</sup>, Zifeng Lu<sup>13</sup>, David G. Streets<sup>13</sup>

[1] {Atmospheric Chemistry and Dynamics Laboratory, NASA Goddard Space Flight Center, Greenbelt, Maryland, US }

[2] {Air Quality Research Division, Environment Canada, Toronto, Canada }

[3] {Earth System Science Interdisciplinary Center, University of Maryland, College Park, US }

[4] {GESTAR, Universities Space Research Association, Columbia, Maryland, US }

[5] {Science Systems and Applications, Inc., Lanham, Maryland, US }

[6] {Applied Physics Laboratory, Johns Hopkins University, Laurel, Maryland, US }

[7] {SRI International, Menlo Park, California, US }

[8] {Meteorology and Air Quality Group, Wageningen University, The Netherlands }

[9] {Royal Netherlands Meteorological Institute, De Bilt, The Netherlands }

[10] {Department of Applied Physics, Eindhoven University of Technology, Eindhoven, the Netherlands }

[11] {University of Technology Delft, Delft, the Netherlands }

[12] {Department of Atmospheric and Oceanic Science, University of Maryland, College Park, Maryland, USA }

[13] {Energy Systems Division, Argonne National Laboratory, Argonne, IL, USA }

Correspondence to: N. A. Krotkov (Nickolay.A.Krotkov@nasa.gov)

## Abstract

The Ozone Monitoring Instrument (OMI) onboard NASA's Aura satellite has been providing global observations of the ozone layer and key atmospheric pollutant gases, such as nitrogen dioxide (NO<sub>2</sub>) and sulfur dioxide (SO<sub>2</sub>), since October 2004. The data products from the same instrument provide consistent spatial and temporal coverage and permit the study of anthropogenic and natural emissions on local-to-global scales. In this paper we examine changes in SO<sub>2</sub> and NO<sub>2</sub> over some of the world's most polluted industrialized regions during the first decade of OMI observations. In terms of regional pollution changes, we see both upward and downward trends, sometimes in opposite directions for NO<sub>2</sub> and SO<sub>2</sub>, for the different study areas. The trends are, for the most part, associated with economic and/or technological changes in energy use, as well as regional regulatory policies. Over the eastern US, both NO<sub>2</sub> and SO<sub>2</sub> levels decreased dramatically from 2005 to 2015, by more than 40% and 80%, respectively, as a result of both technological improvements and stricter regulations of emissions. OMI confirmed large reductions in SO<sub>2</sub> over eastern Europe's largest coal power plants after installation of flue gas desulfurization devices. The North China Plain has the world's most severe SO<sub>2</sub> pollution, but a decreasing trend has been observed since 2011, with about a 50% reduction in 2012-2015, due to an economic slowdown and government efforts to restrain emissions from the power and industrial sectors. In contrast, India's SO<sub>2</sub> and NO<sub>2</sub> levels from coal power plants and smelters are growing at a fast pace, increasing by more than 100% and 50%, respectively, from 2005 to 2015. Several SO<sub>2</sub> hot spots observed over the Persian Gulf are probably related to oil and gas operations and indicate a possible underestimation of emissions from these sources in bottom-up emission inventories. Overall, OMI observations have proved to be very valuable in documenting rapid changes in air quality over different parts of the world during the last decade. The baseline established during the first 11 years of OMI is indispensable for the interpretation of air quality measurements from current and future satellite atmospheric composition missions.

## 1 Introduction

Sulfur dioxide (SO<sub>2</sub>) and nitrogen dioxide (NO<sub>2</sub>) are reactive, short-lived atmospheric trace gases with both anthropogenic and natural sources. Major sources of NO<sub>x</sub> (NO<sub>x</sub> = NO + NO<sub>2</sub>) include fossil fuel combustion, biomass burning, soil emissions (Vinken et al., 2014b), and lightning (Schumann and Huntrieser, 2007). NO<sub>2</sub> participates in the nitrogen cascade of air – water – soil

(EPA, 2011; Galloway et al., 2013), affects atmospheric oxidation rates (Valin et al., 2013), and contributes to surface ozone production (Duncan et al., 2010; Seinfeld and Pandis, 1998). The principal sources of  $\text{SO}_2$  are volcanic and anthropogenic emissions from burning sulfur-contaminated fossil fuels and the refinement of sulfide ores. Volcanic  $\text{SO}_2$  is often injected into the atmosphere at high altitudes above the planetary boundary layer (PBL), while anthropogenic  $\text{SO}_2$  emissions are predominantly in or slightly above the PBL. Chemical reactions in the PBL involving  $\text{SO}_2$  and  $\text{NO}_2$  lead to the production of sulfate and nitrate aerosols, and tropospheric ozone (Seinfeld and Pandis, 1998). Volatile Organic Compounds (VOCs) oxidize in the presence of  $\text{NO}_x$  and sunlight to form ozone ( $\text{O}_3$ ), a major tropospheric pollutant and greenhouse gas (EPA, 2013), and the oxidation product of  $\text{NO}_2$ , nitric acid ( $\text{HNO}_3$ ), reacts with ammonia ( $\text{NH}_3$ ) to form ammonium nitrate aerosols.  $\text{SO}_2$  is oxidized in gas-phase reactions with the hydroxyl radical ( $\text{OH}$ ) or in aqueous-phase reactions with  $\text{O}_3$  or hydrogen peroxide ( $\text{H}_2\text{O}_2$ ) to form sulfate aerosols. Sulfate and nitrate aerosols contribute to fine particulate matter pollution with aerodynamic diameters less than  $2.5\mu\text{m}$  ( $\text{PM}_{2.5}$ ).  $\text{PM}_{2.5}$  poses serious health concerns (Lee et al., 2015; Liu et al., 2015), degrades visibility, causes acidification of water and the biosphere with adverse effects on plants and soil, and impacts weather and climate through direct radiative forcing and indirectly modifying cloud formation and optical properties (IPCC Working Group 1 et al., 2013; Twohy, 2005).  $\text{SO}_2$ ,  $\text{NO}_2$ , and their oxidation products,  $\text{O}_3$  and  $\text{PM}_{2.5}$ , are designated Criteria Pollutants (European Commission, 2015; US EPA, 2016). Space-based characterization of these pollutants enables global, consistent monitoring, which is independent from ground-based measuring networks.

The first space-based quantitative data on  $\text{SO}_2$  mass in volcanic clouds after a major eruption (El Chichón, 1982) was obtained from NASA's Nimbus-7 Total Ozone Mapping Spectrometer (TOMS) (Krueger, 1983). The TOMS  $\text{SO}_2$  detection sensitivity was limited by the instrument's six narrow wavelength bands. In practice, only exceptionally strong anthropogenic  $\text{SO}_2$  signals could be detected, such as those produced by Norilsk smelting plants in Russia or from an accidental combustion of elemental sulfur ( $\text{S}$ ) at the Al-Mishraq State Sulfur Mine Plant in Iraq (Carn et al., 2004; US Department of Veterans Affairs, 2015). Greatly improved sensitivity was demonstrated through detection of  $\text{SO}_2$  emissions from coal-fired power plants using ESA's Global Ozone Monitoring Experiment (GOME, 1995-2005) (Burrows et al., 1997; Eisinger and Burrows, 1998) and SCanning Imaging Absorption spectrometer for Atmospheric

CHartographY, (SCIAMACHY, 2002-2012) (Bovensmann et al., 1999) hyperspectral UV spectrometers. The first tropospheric NO<sub>2</sub> quantification was demonstrated using GOME and SCIAMACHY visible data (Leue et al., 2001; Martin et al., 2002; Richter and Burrows, 2002; Richter et al., 2005). These sensors needed several days to acquire a contiguous global map. The Ozone Monitoring Instrument (OMI) is the first satellite hyperspectral UV/Visible spectrometer with a push broom CCD detector and a 2600 km wide swath (Levelt et al., 2006b), enabling daily, global contiguous mapping of ozone and other trace gases, including SO<sub>2</sub> and NO<sub>2</sub> (Levelt et al., 2006a). OMI was launched in July 2004 on NASA's Aura sun-synchronous afternoon equator crossing polar satellite (Schoeberl et al., 2006) and continues measurements through its 12<sup>th</sup> year, providing the longest data record currently available.. NO<sub>2</sub> and SO<sub>2</sub> observations are also made by two GOME-2 instruments on EUMETSAT's MetOp-A (2006) and B (2012) operational polar satellites (Callies et al., 2000; Richter et al., 2011; Rix et al., 2012; Valks et al., 2011) and Ozone Mapping and Profiler Suite (OMPS) on board the NOAA/NASA Suomi NPP satellite (Dittman et al., 2002; Flynn et al., 2014; Seftor et al., 2014), which have coarser spatial resolutions and higher detection thresholds for emissions from point sources (Fioletov et al., 2013). ESA's next-generation Sentinel series will provide higher spatial resolution and greater sensitivity to SO<sub>2</sub> and NO<sub>2</sub> sources (Ingmann et al., 2012; Veefkind et al., 2012).

In the PBL, both SO<sub>2</sub> and NO<sub>2</sub> have short lifetimes (< 1 day during the warm season) and are concentrated near their emission sources. This facilitates space-based detection of SO<sub>2</sub> and NO<sub>2</sub> sources and global characterization of their spatiotemporal variability (van der A et al., 2006, 2008; Burrows et al., 1999; Castellanos and Boersma, 2012; Eisinger and Burrows, 1998; Fioletov et al., 2013; de Foy et al., 2009; Hayn et al., 2009; He et al., 2012; Hilboll et al., 2013; Huang et al., 2013; Khokhar et al., 2005; Kim et al., 2009; Krotkov et al., 2008; Martin, 2008; Martin et al., 2002; Mijling et al., 2009; Richter et al., 2005; Russell et al., 2012; Schneider and Van Der A, 2012; Theys et al., 2015; Valks et al., 2011; Zhou et al., 2009, 2012) and near-surface concentrations (Duncan et al., 2014; Lamsal et al., 2008, 2010, 2015; McLinden et al., 2014, 2016). Furthermore, over polluted regions satellite observable SO<sub>2</sub> and NO<sub>2</sub> vertically integrated number density profiles (columns) are highly correlated with underlying emissions, allowing space-based (i.e., "top-down") inference of spatial and temporal changes in emissions (van der A et al., 2008; Boersma et al., 2008, 2015; Carn et al., 2007; Ding et al., 2015; Duncan et al., 2013; Fioletov et al., 2011, 2015; de Foy et al., 2014, 2015; Frost et al., 2006; Ghude et al.,

2010, 2013; Hayn et al., 2009; He et al., 2012; Kim et al., 2009; Konovalov et al., 2006, 2010; Lamsal et al., 2011; Lee et al., 2011; Li et al., 2010; Lu et al., 2013, 2015; Martin, 2008; McLinden et al., 2012, 2014; Miyazaki et al., 2012; Napelenok et al., 2008; Reuter et al., 2014; Stavrakou et al., 2008; Streets et al., 2013; Vinken et al., 2014a, 2014b; Zhang et al., 2007), lifetime (Beirle et al., 2011; Fioletov et al., 2011, 2015; de Foy et al., 2015; McLinden et al., 2012), physicochemical conversion (Duncan et al., 2010; Valin et al., 2013) and deposition of these species (Nowlan et al., 2014). OMI has been at the forefront of these rapid advances.

Previous OMI studies focused on specific species, emission sources and regions (van der A et al., 2008; Ahmad et al., 2007; Beirle et al., 2011; Boersma et al., 2011, 2015; Castellanos et al., 2014; Ding et al., 2015; Duncan et al., 2013; Fioletov et al., 2015, 2011; de Foy et al., 2009, 2015; Ghude et al., 2013; Lamsal et al., 2008, 2011, 2015; Lelieveld et al., 2015; Lu et al., 2013; McLinden et al., 2014, 2016; Mebust and Cohen, 2014; Mijling and Van Der A, 2012; Mijling et al., 2009; Russell et al., 2012; Valin et al., 2013; Vinken et al., 2014a, 2014b; Zhou et al., 2012). While NO<sub>2</sub> and SO<sub>2</sub> are both dominated by anthropogenic emissions in polluted regions, the origin of their anthropogenic sources differs, as well as the cost and efficacy of their respective emission control techniques. The often different regional trends and abundances of NO<sub>2</sub> and SO<sub>2</sub> offer valuable insights into energy infrastructures as well as pollution control policies (Li et al., 2010; McLinden et al., 2014). In this paper we examine changes in both SO<sub>2</sub> and NO<sub>2</sub> over the world's most polluted regions during the first decade of OMI observations. Section 2 briefly summarizes OMI SO<sub>2</sub> and NO<sub>2</sub> algorithms and products. Section 3 describes regional SO<sub>2</sub> and NO<sub>2</sub> changes for the world's industrial regions with large SO<sub>2</sub> emissions from coal burning power plants and industries (Fig.1). For these regions we update the previously published OMI trend studies (Duncan et al., 2013; Fioletov et al., 2011; Lu et al., 2013; Russell et al., 2012) and provide a context for a more detailed analysis of individual sources (Duncan et al., 2016; Fioletov et al., 2016; Lu et al., 2015).

## **2 OMI standard SO<sub>2</sub> and NO<sub>2</sub> products**

OMI is the result of a partnership between NASA and the Dutch and Finnish meteorological institutes and space agencies (Levelt et al., 2006b) and flies on the NASA EOS-Aura satellite (Schoeberl et al., 2006). It measures sunlight backscattered from the Earth over a wide range of

1 Ultraviolet (UV) and visible (Vis) wavelengths to derive abundances of ozone and other trace  
2 gases important for air quality and climate. The measurements of SO<sub>2</sub> and NO<sub>2</sub> are both explicit  
3 objectives of the Aura OMI mission (Levelt et al., 2006a) that are aimed at advancing our  
4 understanding of the sources and transformation processes of these pollutants and enabling the  
5 application of OMI data to inform public policy (Streets et al., 2013). Compared with other  
6 satellite UV-Vis instruments, OMI has the highest spatial resolution, least degradation and the  
7 longest record, allowing improved space-borne estimation of NO<sub>2</sub> and SO<sub>2</sub> emissions and the  
8 study of their temporal behavior (Carn et al., 2007; Castellanos and Boersma, 2012; Duncan et  
9 al., 2013; Fioletov et al., 2011, 2013; de Foy et al., 2009; Lamsal et al., 2015; Lu et al., 2013;  
10 McLinden et al., 2012; Zhou et al., 2012).

11 Aura has a local equator crossing time of approximately 13:45 in the ascending node, and  
12 provides nearly global coverage each day. The OMI detector is a 2-dimensional Charge-Coupled  
13 Device (CCD) array. The instrument optics is designed such that the spatial dimension of the  
14 detector is oriented across the orbit track, with an 115° field of view, while the other dimension  
15 records spectral information. Three separate detectors (Dobber et al., 2006; Levelt et al., 2006b),  
16 designated UV-1, UV-2, and Vis, have spectral coverage (full performance) in the ranges of  
17 270–310 nm (spectral resolution, full width at half maximum (FWHM), of 0.63 nm), 310–365  
18 nm (0.45 nm), and 365–500 nm (0.63 nm), respectively. The OMI SO<sub>2</sub> product uses spectral  
19 measurements between 310.5 nm and 340 nm in the UV-2 (Li et al., 2013) and the NO<sub>2</sub> product  
20 uses spectral measurements between 405 nm and 465 nm in the Vis region (Boersma et al., 2011;  
21 Bucsela et al., 2013). The spatial dimension of both detectors is divided into 60 cross-track fields  
22 of view (FOV) corresponding to the specific binned CCD detector rows, such that rows 1 and 60  
23 correspond to the western and eastern edges of the swath, respectively. Spectral measurements  
24 are made over 2-second exposure intervals. This results in along-track coverage of 13 km and  
25 cross-track coverage of 24 km for the near-nadir FOVs (CCD rows about 30). During each orbit,  
26 a total of about 1640 exposures are recorded on the sunlit side of the Earth. The width of the  
27 swath (2600km) is such that 14-15 orbits per day are required to observe the entire surface of the  
28 Earth, although with increased FOV size at the swath edges. Beginning in 2007, some cross-  
29 track positions of the OMI swath were affected by FOV blockage and scattered light, also known  
30 as the “row anomaly” (KNMI, 2012). Here we use only unaffected OMI cross track FOVs

throughout the entire mission, also excluding large FOVs at the edge of the swath, thus considering only the values for CCD rows 6-23.

## 2.1 Retrieval of PBL SO<sub>2</sub>

The original OMI PBL SO<sub>2</sub> product employed the band residual difference (BRD) algorithm, which used only 4 discrete wavelengths (Krotkov et al., 2006). The BRD product is sensitive to the large SO<sub>2</sub> point sources, but has a high noise level (Krotkov et al., 2008) and systematic artifacts that required empirical corrections (Fioletov et al., 2011; Lee et al., 2009). In 2014, a new PBL SO<sub>2</sub> product was released, in which SO<sub>2</sub> is retrieved with a new algorithm that employs a principal component analysis (PCA) technique applied to OMI radiances (Li et al., 2013). Using a clear sky Air Mass Factor (AMF) similar to the previous SO<sub>2</sub> product, but with the full spectral content between 310.5 nm and 340 nm, the PCA algorithm reduces retrieval noise by a factor of two (Li et al., 2013). Recently, the Differential Optical Absorption Spectroscopy (DOAS) SO<sub>2</sub> algorithm developed for the Sentinel 5 Precursor (TROPOMI) has been applied to the OMI radiances and compared with the operational PCA product (Theys et al., 2015). The two products compare well, which lends confidence in OMI SO<sub>2</sub> data. The estimated SO<sub>2</sub> noise is similar between PCA and DOAS algorithms, when using similar assumptions for AMF calculation for pollution SO<sub>2</sub>. However, the DOAS SO<sub>2</sub> algorithm requires empirical corrections to remove background bias.

In this study we will use the OMI operational PCA PBL SO<sub>2</sub> product, which contains the vertical column density (VCD) in Dobson Units (1 DU=  $2.69 \times 10^{16}$  molecules cm<sup>-2</sup>). The product (OMSO2 v1.2.0) is publicly available from the NASA Goddard Earth Sciences (GES) Data and Information Services Center (DISC) ([http://disc.sci.gsfc.nasa.gov/Aura/data-holdings/OMI/omso2\\_v003.shtml](http://disc.sci.gsfc.nasa.gov/Aura/data-holdings/OMI/omso2_v003.shtml)). For background areas the estimated 1 $\sigma$  noise is ~0.5 DU ( 1 DU=  $2.69 \times 10^{16}$  molecules cm<sup>-2</sup> ) over tropical oceanic areas (Li et al., 2013). If we assume that the noise is random and that there are about 100 cloud-free samples per year, the detection limit over low latitudes is estimated to be 4 times the mean error: ~ 0.2 DU for the annual mean. For a single retrieval over polluted areas, random error due to instrument noise is typically on the order of 50-100%. The systematic uncertainties due to our use of fixed Jacobians are 50-100% for cloud-free scenes. The total error for a single retrieval is 70-150%. For an annual average the uncertainties due to the retrieval noise are reduced to the level of 10-15% of the actual signal,

and become insignificant relative to the systematic errors. The systematic errors could be further reduced to the level of 20% applying improved local Jacobians (McLinden et al., 2014, 2016). An important advantage of the PCA algorithm is that the bias over background regions (where SO<sub>2</sub> columns are below the OMI detection limit) is sufficiently small (< 0.1 DU) that it requires no empirical background correction, as applied in other satellite SO<sub>2</sub> algorithms (e.g., Fioletov et al., 2013; Theys et al., 2015). The improved data quality, combined with the pixel averaging and oversampling techniques (e.g., de Foy et al., 2009; Fioletov et al., 2011, 2013, 2015; Lu et al., 2013; McLinden et al., 2014, 2016), provides greatly enhanced sensitivity to anthropogenic SO<sub>2</sub> sources near the surface (Fioletov et al., 2016; McLinden et al., 2014). It has been demonstrated that US SO<sub>2</sub> point sources (e.g., power plants, smelters) with emissions rates as low as ~30-40 kt y<sup>-1</sup> can be detected and analyzed using the PCA OMI SO<sub>2</sub> product (Fioletov et al., 2015). This limit is substantially lower than that reported (70 kt y<sup>-1</sup>) for the previous version OMI SO<sub>2</sub> data (Fioletov et al., 2011).

## 2.2 Retrieval of tropospheric NO<sub>2</sub>

There are two algorithms used operationally to determine tropospheric NO<sub>2</sub> VCDs: the NASA standard product (SP, version 2.1) and the KNMI Dutch-OMI-NO<sub>2</sub> (DOMINO) algorithm (TM4NO2A, version 2, <http://www.temis.nl/airpollution/no2.html>) (Boersma et al., 2011). Both products share a common DOAS spectral fitting of the OMI-measured, sun-normalized backscattered radiances to laboratory-measured absorption spectra of NO<sub>2</sub>, H<sub>2</sub>O, and O<sub>3</sub>, and a calculated Ring pseudo absorption spectrum (Chance and Spurr, 1997), to give NO<sub>2</sub> slant column densities (SCDs). The estimated 1σ noise is ~10<sup>15</sup> molecules cm<sup>-2</sup> or ~10% of the measured SCD over polluted regions (Boersma et al., 2011). The SCDs, after subtraction of the stratospheric contribution are converted to tropospheric VCDs by applying AMFs interpolated from the Look-up-Tables (LUT) with OMI-measured input parameters such as viewing geometry, climatological surface reflectivity, cloud pressure and cloud radiance fraction, assuming *a priori* NO<sub>2</sub> vertical profile shapes. The NASA and KNMI algorithms differ in how they remove the stratospheric contribution and use different *a priori* tropospheric NO<sub>2</sub> profile shapes in the AMF calculation. DOMINO subtracts stratospheric SCD as determined in a data assimilation system, in which the measured SCDs are assimilated with the TM4 chemical transport model (Boersma et al., 2011). The SP estimates stratospheric NO<sub>2</sub> from OMI data without using stratospheric chemical transport models directly. The AMFs are calculated with *a priori* NO<sub>2</sub> monthly mean



vertical profile shapes from the NASA GMI model (Bucsela et al., 2013). Despite the differences, both algorithms produce statistically similar regional trends (see Supplementary Material Fig. S1). Here we use the SP tropospheric NO<sub>2</sub> VCD product version 2.1 publicly available from NASA GES DISC at [http://disc.sci.gsfc.nasa.gov/Aura/data-holdings/OMI/omno2\\_v003.shtml](http://disc.sci.gsfc.nasa.gov/Aura/data-holdings/OMI/omno2_v003.shtml). Over polluted areas the total errors in OMI tropospheric NO<sub>2</sub> VCDs are typically less than 20% for cloud-free FOVs, as confirmed by validation studies employing *in-situ* and remotely sensed data (Bucsela et al., 2013; Irie et al., 2012; Lamsal et al., 2015; Oetjen et al., 2013).

### 2.3 Postprocessing of NO<sub>2</sub> and SO<sub>2</sub> data

For this study, level 2 (L2) tropospheric NO<sub>2</sub> and PBL SO<sub>2</sub> VCDs are gridded at different ground resolutions after excluding FOVs possibly affected by the 1) row anomaly; 2) snow; 3) transient volcanic SO<sub>2</sub> clouds (Appendix A); 4) cloudy scenes with cloud radiance fraction, CRF > 0.5 for NO<sub>2</sub> or CRF > 0.2 for SO<sub>2</sub>. We note that the CRF is approximately twice as larger as the effective cloud fraction derived assuming Mixed Lambert-Equivalent Reflectivity (MLER) cloud model (Boersma et al., 2011; Bucsela et al., 2013; Stammes et al., 2008). Given the very small CRF thresholds, the remaining cloud related errors were estimated to be less than 20% (Lee et al., 2009; McLinden et al., 2014). However, by selecting mostly clear sky conditions, our sampling of the OMI dataset may introduce a bias relative to all-sky conditions (Geddes et al., 2012; McLinden et al., 2014). Clouds are also associated with certain weather conditions, which in turn may affect the level of pollution. These factors may introduce biases in our derived trends in SO<sub>2</sub> and/or NO<sub>2</sub>, but only if there is significant, long-term shift in weather regimes. However, for polluted regions in Fig.1 satellite derived regional trends in cloud reflectivity (less than +/- 2% per decade (Herman et al., 2013) ) are much smaller than those caused by changes in emissions (see section 3).

The standard gridded (0.25° × 0.25°) level 3 (L3), filtered, monthly regional mean values are used in time series analyses following Lamsal et al. (2015) (Appendix B). The L3 data are publicly available from NASA GES DISC archive at <http://disc.sci.gsfc.nasa.gov/Aura/data-holdings/OMI>. We also use L2 (pixel level) data oversampled at higher resolutions (0.01° × 0.01° for NO<sub>2</sub> and 0.02° × 0.02° for SO<sub>2</sub>) to create global and regional maps that highlight point pollution sources. The regional maps are created directly from pre-filtered L2 data by averaging

all OMI pixels within 20 km smoothing radius (30 km for SO<sub>2</sub>) for 3 year time periods. Unlike previous studies (Lee et al., 2009; Fioletov et al., 2011, 2013; Lu et al., 2013; McLinden et al., 2014), no empirical background correction was applied to the PBL SO<sub>2</sub> data.

### 3 Regional pollution changes and interpretation

Figure 1 shows SO<sub>2</sub> and NO<sub>2</sub> multi-year average maps at the beginning of the OMI mission (2005-2007) over the northern hemisphere. Regionally, population density (Lamsal et al., 2013), type of power generation and fuel used, economic activity, and regulatory policies determine average levels of air pollution. The SO<sub>2</sub> map (Fig. 1a) shows hotspots associated with major coal-fired power plants and industrial activities, such as oil and gas refining and metal smelting. The highest SO<sub>2</sub> is found over industrialized and populated regions in eastern China, as the world's second-largest economy relies on sulfur (S)-rich coal for ~70% of its energy consumption (Klimont et al., 2009; Zhang and Cheng, 2009). Based on bottom-up emission inventories, SO<sub>2</sub> emissions from China were the world's largest, at ~33 Tg SO<sub>2</sub> in 2005 (Lu et al., 2010, 2011). High S coal-fired power plants are the major contributors to the SO<sub>2</sub> over the eastern US (SO<sub>2</sub> emissions 14.5 Tg SO<sub>2</sub> in 2005 (US EPA, 2015)), eastern Europe and India (~6.7 Tg SO<sub>2</sub> (Lu et al., 2011) ). SO<sub>2</sub> is undetectable over the western US and western Europe, where emissions of SO<sub>2</sub> have been relatively small due to a smaller proportion of coal-fired power plants, the low S content of coal, and installation of effective flue gas desulfurization devices (FDG) capable of capturing more than 95% of SO<sub>2</sub> emissions (US EIA, 2010).

Large SO<sub>2</sub> column amounts are also observed over the Persian Gulf, due to emissions from the oil and gas industry, gas flaring and shipping in the region. Based on a bottom-up SO<sub>2</sub> emission inventory, the total SO<sub>2</sub> emissions from the Middle East in 2005 were ~6 Tg SO<sub>2</sub> (Smith et al., 2011), less than those from India and the US. However, OMI-observed SO<sub>2</sub> columns over the Persian Gulf region are significantly larger than over these two regions. This implies that real SO<sub>2</sub> emissions from the Middle East (particularly in the Persian Gulf) are significantly underestimated in current bottom-up emission estimates.

In addition to anthropogenic SO<sub>2</sub>, volcanic SO<sub>2</sub> is frequently observed over Kamchatka (Russian Federation), Japan, the South Pacific (e.g., Anatahan volcano, Mariana Islands, Mauna Loa, Hawaii), Sicily (Etna), Mexico (Popocatepetel volcano, south of Mexico city), Central

America and Montserrat, West Indies. Although transient volcanic signals were filtered from the PBL SO<sub>2</sub> data (Table A1), the signals from frequently erupting (e.g., Mt. Etna, Popocatepetel) or degassing volcanos remain. Except for Mt. Etna, Iceland volcanoes (Ialongo et al., 2015; Schmidt et al., 2015), and Mt. Popocatepetl (de Foy et al., 2009), most volcanic sources are located in remote locations and do not contribute to the SO<sub>2</sub> in industrial regions considered here (see OMI daily SO<sub>2</sub> maps for the world's volcanic regions at <http://so2.gsfc.nasa.gov>).

The average OMI NO<sub>2</sub> map (Fig.1b) is correlated with the nighttime lights map (Fig.1c), used here as a proxy for population density and energy production (Lamsal et al., 2013). For example, the highest NO<sub>2</sub> levels are observed over the world's most populated and industrialized regions, including eastern China, western Europe, and the eastern US, where local NO<sub>2</sub> "hot spots" coincide with large urban agglomerations (Schneider et al., 2015), power plants (Duncan et al., 2013; de Foy et al., 2015), and industrial complexes. NO<sub>2</sub> tropospheric columns over India and the Middle East are significantly less than those over China, western Europe and the US. This can be explained by low NO<sub>x</sub> emissions, especially from mobile sources, and, partly, by year-round high temperatures, leading to shorter NO<sub>2</sub> lifetimes (Beirle et al., 2011). For example, Indian NO<sub>x</sub> emissions were relatively low, at 5.7 Tg NO<sub>x</sub> in 2005 (Lu and Streets, 2012), whereas those from China and the US were 16.9 Tg NO<sub>x</sub> (Klimont et al., 2009) and 20.4 Tg NO<sub>x</sub> (US EPA, 2015), respectively. Relatively small, but significant, areal NO<sub>2</sub> enhancements over west African forest are caused by seasonal biomass burning NO<sub>x</sub> emissions (Mebust and Cohen, 2014).

The differences between the spatial distributions of NO<sub>2</sub> and SO<sub>2</sub> over the large regions indicated as boxes in Figures 1a and 1b are related to economic activity, fuel types, combustion technology and different regulatory policies. The most abundant source of SO<sub>2</sub> is Pyrite (FeS<sub>2</sub>) and organic S in lower-grade coal as well as liquid fuel, mostly contained in heterocyclic aromatic compounds in oil, which largely accounts for high SO<sub>2</sub> levels over the Persian Gulf from gas flaring and oil refining. Many developed countries have regulated the S content of fuels and also required catalytic exhaust gas processing, resulting in decreased mobile-source NO<sub>x</sub> and SO<sub>2</sub> emissions in exhaust. Regulations are also focused on stack emissions of NO<sub>x</sub> and SO<sub>x</sub> (SO<sub>x</sub> = SO<sub>2</sub> + SO<sub>3</sub>) at point sources, such as power plants and smelters. This, in turn, has driven technological changes upstream to meet regulatory requirements. For example, fluidized-bed

1 combustion technology permits burning at lower temperature, producing less  $\text{NO}_x$ , and  
2 condensed phase chemical capture of S, producing less gaseous  $\text{SO}_x$ . Chemical Loop  
3 Combustion technology uses catalytic oxygenation to oxidize the fuel largely in the absence of  
4  $\text{N}_2$ , again resulting in greatly reduced  $\text{NO}_x$  leaving the combustion chamber. Stack scrubbers  
5 (i.e., flue gas desulfurization devices, FDG) have been widely deployed in Europe and the US, in  
6 particular, for existing plants, to remove  $\text{SO}_2$  and other chemicals—notably mercury—from the  
7 flue gases, in order to meet regulatory standards. However, these changes have yet to be widely  
8 implemented in developing countries.

9 In addition to emissions, meteorology also plays an important role in regional air  
10 pollution, particularly on relatively short time scales (days to months). For midlatitude areas  
11 discussed in this study (the eastern US, eastern China, and eastern Europe), the concentrations of  
12  $\text{SO}_2$  and  $\text{NO}_2$  often exhibit large day-to-day changes. They tend to increase under the relatively  
13 stagnant conditions ahead of a cold front and decrease dramatically after the cold front brings  
14 precipitation and strong winds into the area (Li et al., 2007). On the interannual time scale, the  
15 frequency of cold front passages may be influenced by large-scale circulation patterns such as  
16 the position of the Siberian high for eastern China (Jia et al., 2015), leading to interannual  
17 changes in  $\text{SO}_2$  and  $\text{NO}_2$ . But meteorology probably plays a lesser role in the longer-term trends  
18 that we discuss in this study. For example, given the general trend of weakening surface winds in  
19 the northern hemisphere (Vautard et al., 2010), one would expect both  $\text{SO}_2$  and  $\text{NO}_2$  to increase  
20 over time in China, with constant emissions. While OMI did initially observe growths in both  
21  $\text{SO}_2$  and  $\text{NO}_2$  over China (section 3.3), the different trends between the two gases after 2007  
22 imply that different emission control measures may play a more significant role in OMI-  
23 observed trends. Similarly, the decreasing pollution levels observed over the eastern US (section  
24 3.1) and eastern Europe (section 3.2) can only be explained by a reduction in emissions. As for  
25 tropical areas such as India, the impact of year-to-year fluctuations in OMI  $\text{SO}_2$  and  $\text{NO}_2$  data  
26 caused by meteorological variations is small relative to the observed fast growth in emissions  
27 that occurred over areas with newly built power plants and many cities (section 3.4).

28 Another factor that can potentially affect derived long-term trends is long-term changes  
29 in the vertical profile shape, because our a priori profiles are constant for the entire mission. We  
30 believe that the impacts are relatively minor for OMI measurements, as the boundary layer is

often thick and quite well mixed during OMI overpass time (in local afternoon). Our previous aircraft measurements over northeastern China and the eastern US show that the difference in AMF due to different SO<sub>2</sub> profile shapes over the two regions are very small (within a few percent, see Krotkov et al. 2008 for more detailed discussion).

With this understanding of the influence of different factors on anthropogenic NO<sub>2</sub> and SO<sub>2</sub> columns, we turn, in the remainder of this section, to examining regional decadal trends as seen by OMI measurements. We examine five regions indicated in Fig.1: the eastern US, eastern Europe and Turkey, eastern China, India, and the Middle East, which all have SO<sub>2</sub> and NO<sub>2</sub> sources detectable by OMI. The regions are in different phases of economic development and environmental regulations. We can therefore compare and contrast the trends in SO<sub>2</sub> and NO<sub>2</sub> that have different sources depending on the types of fuels burned, industrial activity, and regulations.

### 3.1 Eastern US

Over the eastern US the highest levels of SO<sub>2</sub> were observed in areas of intense high-S coal combustion for industrial processes and electricity generation, including the Ohio River Valley and SW Pennsylvania (ORV, blue box in Fig. 2). Concentrations are undetectable over the western US where the local coal is intrinsically lower in S and emissions of SO<sub>2</sub> have been relatively small (US EIA, 2010). Prior investigations involving OMI have reported a 40% SO<sub>2</sub> reduction near power plants in the eastern US between 2005 and 2010 (Fioletov et al., 2011). More recent OMI observations (Fig. 2) show that the SO<sub>2</sub> levels continued to drop after 2010 due to both national (e.g., Clean Air Interstate Rule, CAIR (CAIR, 2009)) and state regulations, such as 2005 Maryland Healthy Air Act (HAA) (He et al., 2016). Currently, US regional SO<sub>2</sub> levels are at or below the OMI SO<sub>2</sub> detection limit of ~0.2 DU. The dramatic decrease over the course of the first 11 years of the OMI mission (Fig. 2) closely matches trends in reported SO<sub>2</sub> emissions (US EPA, 2015) and sulfate deposition ( -5%/yr decrease over the eastern US from 2000-2010 (Hand et al., 2012; Solomon et al., 2014) ) and has also been observed from surface and aircraft measurements (He et al., 2016). This striking improvement in SO<sub>2</sub> coincides with implementation of control technology, such as flue gas desulfurization (FGD), closure of some of the oldest coal power plants and fuel switching from coal to natural gas. Reductions in SO<sub>2</sub> emissions are required by the 1990 Clean Air Act Amendments (CAAA, 1990) and other

1 regulations. Substantial success has been achieved through market-based cap and trade programs  
2 such as the Acid Rain Program (ARP, 2010) and The Clean Air Interstate Rule (CAIR, 2009).  
3 These allow electricity producers to pick the most economical emission control methods. The  
4 conversion to natural gas with much less fuel S than coal has also contributed to the reduction in  
5 SO<sub>2</sub> pollution.

6 Unlike SO<sub>2</sub>, which originates primarily from fuel-bound S, all high-temperature  
7 combustion, including internal combustion engines, can generate NO<sub>x</sub>. As expected, OMI NO<sub>2</sub>  
8 columns peak over major cities and highways, as well as over clusters of power plants. Chicago,  
9 Atlanta, and the megalopolis from Washington, DC to New York, also called the I-95 corridor  
10 (red box in Fig.2), stand out. At the beginning of the OMI mission in 2005, a broad background  
11 of elevated NO<sub>2</sub> was detected over rural areas of the eastern US underlying the hot spots over  
12 large metropolitan areas (Fig. 2). Since that time, NO<sub>2</sub> has significantly decreased as a result of  
13 emission regulations on power plants and cars (Duncan et al., 2013; Lamsal et al., 2015; Lu et  
14 al., 2015; Russell et al., 2012). Decreases in NO<sub>2</sub> are evident in OMI NO<sub>2</sub> data over all major  
15 cities (Lu et al., 2015; Tong et al., 2015), especially over the I-95 corridor (red box in Fig. 2 and  
16 Fig. S1). NO<sub>2</sub> from clusters of power plants has also decreased (e.g., ORV, blue box in Fig. 2). In  
17 general, downward trends in OMI NO<sub>2</sub> data near US power plants correlate well with trends in  
18 NO<sub>x</sub> emissions from the Continuous Emissions Monitoring System (CEMS) (Duncan et al.,  
19 2013) and with surface NO<sub>2</sub> concentrations reported by EPA Air Quality Systems (AQS)  
20 (Lamsal et al., 2015; Lu et al., 2015; Tong et al., 2015). The NO<sub>2</sub> reductions are due to selective  
21 catalytic reduction (SCR) on point sources and three-way catalytic converters on vehicles  
22 (Russell et al., 2012).

23 Fig. 3 (upper row) compares year-to-year changes in the OMI SO<sub>2</sub> and NO<sub>2</sub> annual  
24 columns and bottom-up emissions from power plants over the ORV region (blue box in Fig. 2)  
25 with other heavily polluted regions discussed later. Overall, between 2005 and 2015 the SO<sub>2</sub>  
26 drop over ORV was close to 80%, while NO<sub>2</sub> dropped by 40%, the largest reductions seen in this  
27 study. Previous studies demonstrate a linear ~1:1 relationship between the percent change in NO<sub>x</sub>  
28 or SO<sub>2</sub> emissions from isolated power plants and the corresponding changes in OMI columns  
29 (Fioletov et al., 2011, 2015; de Foy et al., 2015). However, Duncan et al. (2013) show that most  
30 power plants, such as in the eastern US, are co-located with mobile NO<sub>x</sub> sources, so that this

1 relationship is not always obvious. Indeed, OMI observed smaller drop in NO<sub>2</sub> columns (~40%)  
2 than would have been expected from ~60% reduction in NO<sub>x</sub> emissions from the power plants in  
3 the region (Fig. 3).

4 The magnitude of the relative reduction in NO<sub>2</sub> over the I-95 corridor is similar to that  
5 over the ORV (SM: Fig. S1), suggesting similar reduction in NO<sub>x</sub> emissions from cities and  
6 mobile sources. Independent analysis of OMI NO<sub>2</sub> data confirmed that NO<sub>x</sub> emissions of 35  
7 major US urban areas decreased by ~50% from 2006 to 2013 (Lu et al., 2015). We also note the  
8 faster decline in NO<sub>2</sub> levels before 2009 because of the installation of NO<sub>x</sub> emission control  
9 devices (ECDs) on power plants and impact of the economic recession in 2007-2009. Power  
10 plants that were already operating ECDs during the ozone season began operating them year-  
11 round (Lamsal et al., 2015). The annual reduction rate in NO<sub>2</sub> has slowed since 2009 as the US  
12 economy has recovered from the recession and the implementation of further pollution controls  
13 has slowed.

14 Although both SO<sub>2</sub> and NO<sub>2</sub> are Criteria Pollutants, and there remain jurisdictions in the  
15 US in violation of the National Ambient Air Quality Standards (NAAQS) for these primary  
16 pollutants, just as important is their role as precursors of key secondary air pollutants such as fine  
17 particles (PM<sub>2.5</sub>) and ozone. The greatest numbers of Americans at risk for harmful effects of air  
18 pollution are subject to exposure to these secondary pollutants (Lee et al., 2015). By 2015, total  
19 US SO<sub>2</sub> emissions fell to about 1/6 of their 1970 peak, but NO<sub>x</sub> emissions only fell substantially  
20 after 2000 and are now about ½ of their peak in 2000 (<http://www.epa.gov/ttnchie1/trends/>).  
21 Because of these NO<sub>x</sub> reductions, photochemical smog over eastern US has improved  
22 significantly over the same time period (Castellanos et al., 2011; Hogrefe et al., 2011; Simon et  
23 al., 2015). The total deposition of oxidized N (the combination of wet and dry deposition of  
24 species such as NO<sub>2</sub> and NO<sub>3</sub><sup>-</sup>) has improved as well (Nowlan et al., 2014) indicating that the  
25 efforts to control NO<sub>x</sub> emissions have been successful. As result of larger SO<sub>2</sub> reductions, the  
26 SO<sub>2</sub>/NO<sub>2</sub> column ratio dropped over the ORV region from its maximal values of ~4-5 in 2005 to  
27 less than 2 in 2012 (SM, Fig. S2). We expect similar change in PM speciation with increasing  
28 relative contribution of nitrate aerosols.

### 3.2 Eastern Europe

Europe experienced a ~80% reduction in SO<sub>2</sub> emissions between 1990 and 2011 (EEA, 2013). Particularly, in western Europe, after significant reduction of SO<sub>2</sub> emissions in the 1980s-1990s, the SO<sub>2</sub> levels have dropped below the OMI detection limit of ~0.2 DU. There are, however, detectable SO<sub>2</sub> sources in eastern Europe (Fig. 4). The spatial distribution of the observed SO<sub>2</sub> columns at the beginning of OMI mission is consistent with the spatial pattern of SO<sub>2</sub> concentrations derived from the surface monitoring stations for 2005 (Denby et al., 2010). Notable anthropogenic SO<sub>2</sub> sources include, for example, the mining and industrial districts in Donbass region in Eastern Ukraine, large coal-fired thermal power plants around the Sea of Marmara and those near Kahramanmaras in southern Turkey, as well as those near Galabovo in Bulgaria, Gorj County in southwestern Romania, Belgrade in Serbia, and Megalopoli in southern Greece (Fioletov et al., 2016). Most of SO<sub>2</sub> hot spots are due to use of local high *S* lignite (brown) coal for power generation and incomplete SO<sub>2</sub> removal from the flue gas. Fig. 3 (second row) shows interannual variations in SO<sub>2</sub> and NO<sub>2</sub> columns over the Maritsa Iztok power complex in Stara Zagora, Bulgaria (see blue box in Fig. 4). Large SO<sub>2</sub> reductions (~50%) between 2011 and 2015 are consistent with the installation of FGD, while NO<sub>2</sub> remains approximately constant, suggesting stable electricity production. Another important source of SO<sub>2</sub> in the region is the Mt. Etna volcano, in Sicily. OMI SO<sub>2</sub> retrievals indicate considerable decreases in SO<sub>2</sub> over Megalopoli, Galabovo, and Gorj County, likely owing to more stringent SO<sub>2</sub> controlling measures on power plant emissions in response to mandates by the European Union. SO<sub>2</sub> emissions from Turkey, on the other hand, have increased during the same period, particularly over Kahramanmaras, where new power plants went into service in 2006 (see <http://globalenergyobservatory.org/geoid/42972>). Increases in SO<sub>2</sub> over Serbia may reflect growth in energy consumption (mainly from coal) as the country's economy recovers from wars in the 1990s.

Fig. 4 (bottom row) gives the spatial distribution of OMI tropospheric NO<sub>2</sub> over eastern Europe, which shows enhanced columns in densely populated and industrial areas. By far the largest NO<sub>2</sub> was observed over Moscow, Russian Federation, confirmed by in situ measurements at different heights within PBL (Chubarova et al., 2009, 2016; Elansky et al., 2007; Gorchakov, 2011). In Moscow maximal surface concentrations exceed 100 ppb for NO<sub>2</sub>, but are less than 2 ppb for SO<sub>2</sub> (Elansky et al., 2007). OMI also observed large NO<sub>2</sub> over industrial regions near



Katowice in south Poland, east Germany and the northwestern Czech Republic. Elevated NO<sub>2</sub> columns are evident over large cities, such as Istanbul, Prague, Warsaw, Vienna, Rome, Athens, and Budapest. These enhancements correlate well with emissions source distribution (Janssens-Maenhout et al., 2015). While road traffic is in general the most important NO<sub>x</sub> source in Europe (EEA, 2013; Vestreng et al., 2009), in some eastern European countries the power sector is the major contributor (Zyrichidou et al., 2013). New construction and upgrades in capacity of older power plants, as well as emission control measures affect NO<sub>2</sub> columns (Castellanos and Boersma, 2012; Zhou et al., 2012). Several studies based on bottom-up emissions and satellite observations have reported substantial decreases in NO<sub>x</sub> emissions and NO<sub>2</sub> columns in most of the western European countries due to stricter emission regulations (Castellanos and Boersma, 2012; Curier et al., 2014; EEA, 2013; Lamsal et al., 2011; Schneider et al., 2015; Vestreng et al., 2009; Zhou et al., 2012). In contrast, changes in emissions are rather small in eastern Europe (Zyrichidou et al., 2010). An increase in NO<sub>x</sub> emissions is reported for those countries where implementation of the European Union (EU) air quality standards is less effective (AQ\_Environment\_EC, 2015; Vestreng et al., 2009). OMI measurements are consistent with previous studies, suggesting small or insignificant NO<sub>2</sub> column trends on a regional level. Changes appear to be country-specific and likely depend on the socio-economic and political situation and legislative abatement measures of the country. The EU air quality standards hold for all EU-countries (including Poland, Hungary, Bulgaria, Croatia, the Baltic States, Slovenia, Slovakia), but not for Serbia, Russia, Ukraine, Belarus, and Turkey. Some countries have asked for a time extension to meet certain standards because several member States have particular difficulties in achieving compliance with the criteria for PM and NO<sub>2</sub>.

### **3.3 Eastern China**

The growth of the Chinese economy over the past two decades has been mainly driven by rapid industrialization and urbanization (Huang et al., 2013) and has been accompanied by large increases in both electricity generation (mainly coal-fired power plants) and the number of vehicles on Chinese roads. As evident in Fig. 1a and 5, China has the world's highest SO<sub>2</sub> emissions, particularly over the high S coal-rich, heavily industrial areas in Hebei, Henan, and Shandong provinces in the North China Plain (NCP, blue box in Fig. 5) and Inner Mongolia (Li et al., 2010; Zhang et al., 2009), the highly populated Sichuan Basin (SB, red box in Fig.5), the megacity clusters around Shanghai (the Yangtze River Delta, YRD – black box in Fig. 5) and

Guangzhou-Hong Kong (the Pearl River Delta, PRD). Similarly, OMI retrievals also reveal much greater  $\text{NO}_2$  over eastern China than other regions of the world (Fig. 1b), especially over NCP, YRD and PRD (Fig. 5). The  $\text{NO}_2$  levels are relatively low over SB, but higher over YRD and PRD. The  $\text{SO}_2/\text{NO}_2$  column ratios were 8-10 over SB, 3-5 over NCP and less than 2 over YRD and PRD in 2005 (Fig. S4). The ratios reflect to some extent the level of modernization in the regions. The PRD and YRD have relatively less coal-fired power plants but higher population and car density, therefore greater  $\text{NO}_2$  relative to  $\text{SO}_2$ .

The overall  $\text{SO}_2$  loading, although still at a relatively high level, has decreased over the years (Fig. 5). This is more clearly shown in the  $\text{SO}_2$  time series in Fig. 3, which suggests that the  $\text{SO}_2$  loading over the NCP peaked in 2007, and has since shown an overall decreasing trend despite relatively large year-to-year variations. The reduction in  $\text{SO}_2$  during 2008-2010 may be attributed to both the economic recession and emission control measures before the 2008 Beijing Olympic Games (Li et al., 2010; Lu et al., 2011; Mijling et al., 2009; Witte et al., 2009). The temporary rebound in 2011 may reflect a resurgence in the economy due to stimulation by the government. This is followed by a dramatic ~60% reduction over the four-year period during 2012-2015 that may be attributed to both stricter emission reduction targets during the 12<sup>th</sup> Five-Year Plan (2010-2015) (Tian et al., 2013; Zhao et al., 2013), more widespread use of FGD on coal-fired power plants and industries, as well as a slowdown in the growth rate of the Chinese economy. We confirmed the 2012-2015  $\text{SO}_2$  reduction over NCP applying our  $\text{SO}_2$  retrievals to the measurements from the Ozone Mapping and Profiler Suite (OMPS) instrument on board NASA-NOAA Suomi National Polar Partnership (SNPP) satellite (Fig. S3). In relative terms the  $\text{SO}_2$  reduction in 2005-2015 was larger over YRD and SB regions compared to NCP (Fig. S3).

$\text{NO}_2$  over NCP, on the other hand, peaked in 2011 after dramatic ~50% increase since 2009 (Fig. 3) and decreased slightly in 2012 and 2013 (Fig. 3). Temporary drop in 2008 can be attributed to strict pollution reduction measures implemented before 2008 Olympic games and economic recession. The reductions were strongest in Beijing, Tianjin and Schijiazhuang regions (Mijling et al., 2009; Witte et al., 2009). The dramatic ~40% drop in  $\text{NO}_2$  in 2014-2015 is likely a result of the slowest economic growth rate for China in nearly 25 years. According to the National Bureau of Statistics, the electricity generation by thermal power plants decreased by several percent in the second half of the year as compared with 2013. Similarly there is also a

slowdown in coal-intensive industrial sectors (Guay, 2015) and stricter emission control policies (MEP, 2013). Independent satellite NO<sub>2</sub> retrievals with GOME-2A, GOME-2B and OMI also confirm large reduction in NO<sub>2</sub> over eastern China between 2013 and 2014 (Richter et al., 2015). Over SB and YRD NO<sub>2</sub> columns peaked in 2010 and remained relatively constant afterwards (Fig. S1). As a result of the different trends between SO<sub>2</sub> and NO<sub>2</sub> the SO<sub>2</sub> to NO<sub>2</sub> ratios dropped to their lowest values of ~2-3, ~1-2 and less than one over SB, NCP and YRD regions, respectively (Fig. S4).

### 3.4 India

Figure 6 shows multi-year mean OMI SO<sub>2</sub> and NO<sub>2</sub> maps over India. A number of SO<sub>2</sub> and NO<sub>2</sub> hot spots are observed, and they match the locations of large coal-fired power plants and major cities (Ghude et al., 2011, 2013). This is because coal-fired power plants are the dominant SO<sub>2</sub> and NO<sub>x</sub> emission sources in India, and they are often built near large cities where other anthropogenic emissions are also high. Fig. 6 also shows that from 2005 to 2015, there was an increase in the OMI-observed SO<sub>2</sub> and NO<sub>2</sub> columns over India, mainly reflecting the fast expansion of the power sector driven by rapid economic growth. Based on an updated unit-based coal-fired power sector database (Lu and Streets, 2012; Lu et al., 2013), the total installed capacity, power generation, and fuel consumption of Indian coal-fired power plants increased dramatically by 126%, 91%, and 93%, respectively, during 2005-2014. The SO<sub>2</sub> emissions from power plants are high, because S in local coal is mostly in organic form and cannot be removed by physical cleaning methods (Lookman and Rubin, 1998).

Unlike the US, Europe, and China, SO<sub>2</sub> and NO<sub>x</sub> emitted from coal-fired power plants are not regulated in India and the installation and operation rates of SO<sub>2</sub> and NO<sub>x</sub> emission control devices are very low. FGD devices for SO<sub>2</sub> were reported to be operating in only three power plants at the beginning of OMI mission (Chikkatur et al., 2007). NO<sub>x</sub> emissions by coal-fired power plants are also not regulated in India. Although some new plants were reported to be equipped with low-NO<sub>x</sub> burners (LNB), the actual installation rate and performance of these LNB devices are not known. Based on bottom-up emission inventories we estimate that SO<sub>2</sub> and NO<sub>x</sub> emissions from Indian coal-fired power plants increased by 103% and 94%, respectively, during 2005-2014 (Lu and Streets, 2012; Lu et al., 2013).

As shown in Fig.3, the growth rates in OMI-observed  $\text{SO}_2$  ( $200\%\pm 50\%$ ) and  $\text{NO}_2$  ( $50\%\pm 20\%$ ) columns during 2005-2015 were particularly large over the industrial regions in Chhattisgarh and Odisha (blue box in Fig. 6), one of India's most active areas in terms of building new power plants. By the end of 2014, the total installed capacity of coal-fired power plants in this region was 28 GW, 85% of which ( $\sim 24$  GW) was installed after 2005, accounting for  $\sim 26\%$  of the total newly installed capacity in India. As a result,  $\text{SO}_2$  and  $\text{NO}_x$  emissions from coal-fired power plants in this region were estimated to increase both by  $\sim 190\%$  from 2005 to 2014 (Lu and Streets, 2012; Lu et al., 2013), largely in line with OMI  $\text{SO}_2$  observations (Fig.3g). India's total annual  $\text{SO}_2$  emissions almost doubled from 6.7 Tg in 2005 to estimated 12 Tg in 2014. In 2014, India has not only surpassed the US to be the world's second largest  $\text{SO}_2$  emitting country, but also has reached more than 40% of the  $\text{SO}_2$  emissions of the world's largest emitter, China.

During the last decade OMI observed much smaller  $\text{NO}_2$  increases ( $\sim 50\%$ ) than one would have expected from the increase in  $\text{NO}_x$  emissions from the coal-fired power plants (Fig. 3h). One possible explanation for the discrepancy might be relatively high  $\text{NO}_2$  background from other emission sources. While coal-fired power plants may be the single largest contributor to  $\text{SO}_2$  in this region, transportation is a larger contributor to  $\text{NO}_x$ , and the slower increase in transportation emissions could have masked the sharp increase in coal-fired power plants  $\text{NO}_x$  emissions. In India, the prevalence of motorcycles with small, two-stroke engines lead to high transportation emission factors for CO, VOC and PM, but produce only modest amounts of  $\text{NO}_x$  (Dickerson, 2002). Also, with a 3-fold increase in  $\text{NO}_x$  emissions from the power plants, there could be some non-linear effects in  $\text{NO}_x$  chemistry, changing the lifetime of  $\text{NO}_2$ . Heavy loadings of soot may also remove  $\text{NO}_2$  (Dickerson, 2002). The discrepancies will be addressed in future studies.

### 3.5 Middle East

In the Middle East, abundant oil and gas deposits supply cheap and relatively clean fuels for electricity generation, water desalination, and industries. OMI detects the largest  $\text{SO}_2$  emissions over the Persian Gulf. The sources for these emissions are apparently not included in the current global emission inventory such as EDGAR-HTAP dataset (Janssens-Maenhout et al., 2015).

1 Based on the most recent SO<sub>2</sub> emission inventory, the total SO<sub>2</sub> emissions from the Middle East  
2 in 2005 were ~6 Tg (Klimont et al., 2013; Smith et al., 2011), less than those from India and the  
3 US. However, OMI observed SO<sub>2</sub> columns over the Gulf region are significantly larger than  
4 those over India and US. That suggests that the real SO<sub>2</sub> emissions from the Middle East  
5 (particularly in the Persian Gulf) may be several times higher than current bottom-up emission  
6 estimates. This is consistent with independent OMI SO<sub>2</sub> retrievals (Theys et al., 2015). Inverse  
7 modeling using OMI and SCIAMACHY retrievals also suggests an underestimate of SO<sub>2</sub>  
8 emissions from the Persian Gulf (Lee et al., 2011).

9 In-situ measurements of SO<sub>2</sub> and other pollutants are rarely reported for the region, but  
10 available data generally indicate significant SO<sub>2</sub> loading over the Persian Gulf. For example, an  
11 aircraft campaign conducted north of the United Arab Emirates during winter 2001 measured  
12 SO<sub>2</sub> concentrations of up to 40 ppb (see [https://www.rap.ucar.edu/asr2002/i-precip\\_physics/precip\\_physics.htm](https://www.rap.ucar.edu/asr2002/i-precip_physics/precip_physics.htm) ), greater than what has been previously observed over  
13 eastern China (Dickerson et al., 2007; He et al., 2012). The largest hotspot observed by the  
14 aircraft, near Zirku Island, also appears to be co-located with a hotspot in OMI retrievals. In  
15 another study, passive sampling of SO<sub>2</sub> at various locations on Khark Island near the north end  
16 of the Gulf during 2003-2004 reported that the SO<sub>2</sub> loading was above the air quality standard  
17 (sometimes by several-fold) most of the time (Pourzamani et al., 2012). These high SO<sub>2</sub> columns  
18 over the Persian Gulf are likely the result of gas flaring activities from offshore oil and natural  
19 gas facilities, although shipping emissions and other sources may also contribute to them. Gas  
20 flaring is used on offshore oil rigs to dispose of gases such as hydrogen sulfide (H<sub>2</sub>S) for safety,  
21 operational, and economic reasons and can have significant impacts on the local and regional  
22 environment in the Middle East.  
23

24 Middle East cities also show SO<sub>2</sub> emissions due to both mobile and stationary sources.  
25 Oil-burning boilers may constitute another important source of SO<sub>2</sub> in cities or population  
26 centers, as implied by the relatively high sulfate (~10 µg m<sup>-3</sup>) that is closely associated with oil  
27 combustion tracers (e.g., vanadium), according to an aerosol source apportionment study for  
28 Kuwait City (Alolayan et al., 2013). The S content in gasoline and diesel is much higher in this  
29 region as compared with others such as Europe, which enforces stricter emission control  
30 measures (see <http://www.unep.org/transport/pcf/PDF/JordanWrkshp->

[MiddleEastFuelQuality.pdf](#)). Some of the largest point SO<sub>2</sub> sources in the region coincide with smelters or oil refineries, such as the Sarcheshmeh Copper Complex in Kerman Province, Iran, which is the largest copper smelter in the Middle East. Fig. 3 (bottom row) show interannual variations in observed SO<sub>2</sub> and NO<sub>2</sub> columns over Persian Gulf (blue box in Fig. 7). Since 2010 SO<sub>2</sub> columns have steadily dropped by ~20%, but increased again in 2014-2015 to 2005 levels. A recent study (Lelieveld et al., 2015) reported that OMI SO<sub>2</sub> over the Persian Gulf increased between 2005 and 2010, and then decreased between 2010 and 2014. Their results are based on retrievals using a different algorithm, but are qualitatively consistent with this study.

OMI-retrieved regional NO<sub>2</sub> levels over the Middle East are much smaller than over China (Fig. 6) and the US (Fig. 2). This may also be the results of the short lifetime of NO<sub>2</sub> in this hot and photochemically active region (Beirle et al., 2011). NO<sub>x</sub> emissions in the region are associated with power generation and mobile sources. Local NO<sub>2</sub> enhancements coincide with heavily populated cities that have high car densities, such as Jerusalem (Israel) and Cairo (Egypt) (Boersma et al., 2009), Tehran (Iran), Kuwait City (Kuwait), Dubai (UAE), Riyadh and Jeddah (Saudi Arabia). In terms of regional trend over the Persian Gulf (blue box in Fig. 7), NO<sub>2</sub> columns increased by ~ 20% between 2005 and 2008, but remained approximately constant afterwards (Fig. 3). For major metropolitan areas in the region, Lelieveld et al. (2015) focused on the reversal of OMI NO<sub>2</sub> trends due to recent air quality regulations and domestic and international conflicts in the region. Their results are, for the most part, qualitatively consistent with Fig. 7. For example, their reported decrease of NO<sub>2</sub> over Damascus, Syria since 2011 (due to civil war) and increase over Baghdad, Iraq since 2007 are also visible in Fig. 7.

## 4 Conclusions

The first decade of OMI observations have yielded profound insights into the spatial distribution and temporal trends in SO<sub>2</sub> and NO<sub>2</sub> pollution around the world. For regions with detailed bottom-up emissions estimates or continuous emissions monitoring, OMI shows generally good agreement with these independent data sources. OMI-derived trends also agree well with those from available in situ measurements and deposition data. This adds confidence to the use of OMI to track locations, changes, and transport patterns of SO<sub>2</sub> and NO<sub>2</sub> over areas of the planet

1 lacking local observations. In many regions pollution levels have changed dramatically reflecting  
2 underlying changes in SO<sub>2</sub> and NO<sub>x</sub> emissions (Fig. 8):

3 1) Over the eastern US, both NO<sub>2</sub> and SO<sub>2</sub> levels decreased dramatically from 2005 to 2015. SO<sub>2</sub>  
4 concentrations over the Ohio River Valley and western Pennsylvania fell by 80%, consistent  
5 with the National Emission Inventory (NEI), which reports a decrease of about 66% for total US  
6 emissions. NO<sub>2</sub> concentrations over the eastern US fell by more than 40%, also consistent with  
7 the NEI trend for emissions from the entire country. The Clean Air Act Amendments and  
8 regulations such as CAIR mandated these emissions reductions, and OMI confirmed their  
9 efficacy.

10 2) Over eastern Europe, OMI observed substantial (more than 50%) SO<sub>2</sub> decreases in the vicinity  
11 of the largest coal-fired power plants, where flue gas desulfurization devices were installed  
12 during the study period. Over some areas including Turkey and Serbia, local SO<sub>2</sub> increased,  
13 perhaps because of increased industrial activity. NO<sub>2</sub> levels in the vicinity of the largest eastern  
14 European power plants in Bulgaria remain constant.

15 3) Over China, the highest SO<sub>2</sub> and NO<sub>2</sub> levels are observed over the North China Plain, with the  
16 highest concentrations in the world. SO<sub>2</sub> peaked in 2007, with a secondary peak in 2011, but by  
17 2015 SO<sub>2</sub> has fallen to half of the levels seen at the beginning of the OMI record in 2005. Total  
18 Chinese electricity production and coal combustion have increased during the same period, and  
19 the observed decrease likely has resulted from centralization of industry and power production  
20 and the implementation of pollution control devices. NO<sub>2</sub> concentrations peaked in 2011, but by  
21 2015 have returned to 2005 levels.

22 4) Over India, despite relatively low levels as compared with China, both SO<sub>2</sub> and NO<sub>2</sub> have  
23 increased, particularly over the northeast, where a large number of newly built coal power plants  
24 have doubled SO<sub>2</sub> while increasing NO<sub>2</sub> by ~50%. This is the fastest increase in pollution  
25 concentrations observed by OMI. In 2014 India has surpassed the US to become the world's  
26 second largest SO<sub>2</sub> emitting country.

27 5) Over the Middle East, OMI detected several SO<sub>2</sub> hot spots with a broad maximum over the  
28 Persian Gulf region. These hotspots are probably related to oil and gas operations but are mostly  
29 absent in bottom-up emission inventories, such as EDGAR. High concentrations of NO<sub>2</sub> are

1 observed over major cities but less so over oil and gas operations. SO<sub>2</sub> shows no discernable  
2 trend over the Gulf while NO<sub>2</sub> rose from 2005 to 2008 and has since remained largely  
3 unchanged.

4 In summary, this study demonstrates that satellite remote sensing from advanced  
5 instruments such as OMI can provide long-term, nearly continuous global monitoring of SO<sub>2</sub> and  
6 NO<sub>2</sub>. Where *in situ* concentration measurements, emission inventories, and deposition  
7 monitoring are available, OMI provides complementary measurements to supplement and verify  
8 those other data sources. OMI can also find unreported or underreported major emissions such  
9 as over the Persian Gulf. OMI SO<sub>2</sub> and NO<sub>2</sub> data can also help to further our understanding of  
10 the production and impact of secondary pollutants such as tropospheric ozone and particulate  
11 matter. Better understanding of these secondary pollutants will help refining satellite SO<sub>2</sub> and  
12 NO<sub>2</sub> retrievals.

13 Space-based monitoring plays an increasingly important role in the science of  
14 tropospheric chemistry and air quality applications to help mitigate anthropogenic and natural  
15 impacts on climate, sensitive ecosystems, and human health. It is essential to continue and  
16 maintain overlapping long-term satellite data records. The baseline established during the first 11  
17 years of OMI is invaluable for the interpretation of measurements from future satellite  
18 atmospheric chemistry missions. The OMI NO<sub>2</sub> and SO<sub>2</sub> data sets used in this study will be  
19 refined and continued by the TROPOspheric Monitoring Instrument (TROPOMI) (Veefkind et  
20 al., 2012), which is planned for launch on ESA's Sentinel 5 Precursor (S5P) satellite in 2016.  
21 TROPOMI will have a significantly higher signal-to-noise and spatial resolution (7km x 7km at  
22 nadir) than OMI; both features are very important for monitoring point pollution sources and  
23 trends. TROPOMI is part of the European Sentinel series that will continue the global pollution  
24 data record for another 20 years (Ingmann et al., 2012). The space-based capabilities for air  
25 quality applications will be further enhanced by the addition of higher-ground resolution hourly  
26 observations from the three geostationary satellites over North America (Tropospheric  
27 emissions: monitoring of pollution (TEMPO), <http://tempo.si.edu>) (Chance et al., 2013), over  
28 Europe (Sentinel 4 UVN (Ingmann et al., 2012)) and East Asia (Geostationary Environment  
29 Monitoring Spectrometer (GEMS) on board the GeoKOMPSAT satellite) (Kim, 2012). This  
30 constellation will allow for unprecedented observations of the key pollutants in the atmosphere.



## Appendix A: Filtering transient volcanic clouds

Days affected by transient volcanic SO<sub>2</sub> signals were excluded as follows. Every day the region-wide 99.9-percentile of SO<sub>2</sub> VCDs was computed. If it was found to exceed a threshold value (Table A1) then all data from that day were excluded. This was found to perform better than a simple maximum SO<sub>2</sub> or NO<sub>2</sub> column cut-off as it tended to remove volcanic signals that, while elevated, would not exceed the maximum. A disadvantage of this method is that, while the volcanic contamination would generally only impact a small portion of the region, all data from that day were removed. The SO<sub>2</sub> threshold employed varied from 5 to 10 DU (table A1) and was chosen by examining the 99.9-percentile time series during known periods of minimal volcanic activity. Different regions were found to be affected differently, a result of their proximity to significant eruptions. For regions that span the northern mid-latitudes such as US, Europe, and China, many of the days occurred in 2008 and 2009 and can be attributed to the eruptions of Kasatochi (Aleutian Islands, Alaska, August 2008, 52N) and Sarychev (Kuril Islands, Eastern Russia, June 2009, 48N). By contrast, the Nabro eruption (northern Africa, June 2011, 13.37N) removed the most days over India and Africa whereas the Middle East appeared to be largely unaffected by volcanic emissions.

## Appendix B: Timeseries analysis

We use standard Level 3 monthly regional mean SO<sub>2</sub> and NO<sub>2</sub> columns and a regression model discussed in Lamsal et al., (2015) to compare inter-annual timeseries for different regions. The time series of monthly average values ( $\Omega$ ) are assumed to be comprised of three additive subcomponents: a seasonal component ( $\alpha$ ), a linear trend component ( $\beta$ ), and residues or noise ( $R$ ) component:

$$\Omega(t) = \alpha(t) + \beta t + R(t), \quad (\text{B1})$$

where,  $t$  represents time (month). The time dependent seasonal regression coefficient ( $\alpha$ ) is given by a constant plus intra-annual sine and cosine harmonic series (Randel and Cobb 1994):

$$\alpha(t) = c_0 + \sum_{j=1}^3 \left( c_{1j} \sin\left(\frac{2\pi jt}{12}\right) + c_{2j} \cos\left(\frac{2\pi jt}{12}\right) \right), \quad (\text{B2})$$

where  $c_0$ ,  $c_{1j}$ , and  $c_{2j}$  are constant coefficients. The major portion of the annual cycle is explained by the seasonal variation of the  $\text{NO}_x$  and  $\text{SO}_2$  lifetime. Other factors, such as monthly variation in source strength, could also affect the annual variation of  $\text{NO}_2$  and  $\text{SO}_2$  columns, but these contributions, especially for  $\text{NO}_2$ , to the seasonal cycle are typically smaller, especially for polluted areas. The seasonal pattern can evolve with time. We identify and extract seasonal and trend components by exploiting changes in the seasonal pattern (amplitude and phase) for individual years. For each year we fit a regression line using monthly observations from that year itself and 6 observations each from adjacent years. This provides a series of local regression lines that incorporate explicit time dependence. Comparison of local regression lines with high- and low-amplitude regression lines allows identification and isolation of two seasonal terms ( $\alpha_1$ ,  $\alpha_2$ , where  $\alpha = \alpha_1 + \alpha_2$  in Eq. 1) and the linear trend ( $\beta$ ) and residues. Since we are interested in interannual changes, we do not explicitly derive linear trend, but rather calculate changes from 2005 from de-seasonalized  $\text{NO}_2$  and  $\text{SO}_2$  columns (Fig. 3).

## Acknowledgements

The authors acknowledge the NASA Earth Science Division for funding of OMI  $\text{SO}_2$  and  $\text{NO}_2$  product development and analysis. The Dutch - Finnish built OMI instrument is part of the NASA's EOS Aura satellite payload. We thank systems engineering, instrument calibration and satellite integration teams for making this mission a success. The OMI project is managed by KNMI and the Netherlands Space Agency (NSO). The authors would like to thank the KNMI OMI team for producing L1B radiance and irradiance data and updating the key calibration data, the operational algorithm for the  $\text{NO}_2$  slant column fitting and performing operations together with the U.S. Aura operations team, as well as OMI SIPS processing team for continuing support. Authors would like to thank two anonymous reviewers for their helpful comments.

## References

- Ahmad, Z., McClain, C. R., Herman, J. R., Franz, B. A., Kwiatkowska, E. J., Robinson, W. D., Bucsela, E. J. and Tzortziou, M.: Atmospheric correction for  $\text{NO}_2$  absorption in retrieving water-leaving reflectances from the SeaWiFS and MODIS measurements., *Appl. Opt.*, 46(26), 6504–6512, doi:10.1364/AO.46.006504, 2007.

1 Alolayan, M. A., Brown, K. W., Evans, J. S., Bouhamra, W. S. and Koutrakis, P.: Source  
2 apportionment of fine particles in Kuwait City., *Sci. Total Environ.*, 448, 14–25,  
3 doi:10.1016/j.scitotenv.2012.11.090, 2013.

4 AQ\_Environment\_EC: Air Quality - Environment - European Commission, [online] Available  
5 from: [http://ec.europa.eu/environment/air/quality/legislation/time\\_extensions.htm](http://ec.europa.eu/environment/air/quality/legislation/time_extensions.htm) (Accessed 18  
6 August 2015), 2015.

7 ARP: Acid Rain Program | Clean Air Markets | US Environmental Protection Agency, EPA  
8 [online] Available from: <http://www.epa.gov/airmarkets/> (Accessed 7 March 2016), 2016.

9 Beirle, S., Boersma, K. F., Platt, U., Lawrence, M. G. and Wagner, T.: Megacity emissions and  
10 lifetimes of nitrogen oxides probed from space., *Science*, 333(6050), 1737–9,  
11 doi:10.1126/science.1207824, 2011.

12 Boersma, K. F., Jacob, D. J., Eskes, H. J., Pinder, R. W., Wang, J. and van der A, R. J.:  
13 Intercomparison of SCIAMACHY and OMI tropospheric NO<sub>2</sub> columns: Observing the diurnal  
14 evolution of chemistry and emissions from space, *J. Geophys. Res. Atmos.*, 113(16),  
15 doi:10.1029/2007JD008816, 2008.

16 Boersma, K. F., Jacob, D. J., Trainic, M., Rudich, Y., Desmedt, I., Dirksen, R. and Eskes, H. J.:  
17 Validation of urban NO<sub>2</sub> concentrations and their diurnal and seasonal variations observed from  
18 the SCIAMACHY and OMI sensors using in situ surface measurements in Israeli cities, *Atmos.*  
19 *Chem. Phys.*, 9(2), 3867–3879, doi:10.5194/acp-9-3867-2009, 2009.

20 Boersma, K. F., Eskes, H. J., Dirksen, R. J., Van Der A, R. J., Veefkind, J. P., Stammes, P.,  
21 Huijnen, V., Kleipool, Q. L., Sneep, M., Claas, J., Leitão, J., Richter, A., Zhou, Y. and Brunner,  
22 D.: An improved tropospheric NO<sub>2</sub> column retrieval algorithm for the Ozone Monitoring  
23 Instrument, *Atmos. Meas. Tech.*, 4(9), 1905–1928, doi:10.5194/amt-4-1905-2011, 2011.

24 Boersma, K. F., Vinken, G. C. M. and Tournadre, J.: Ships going slow in reducing their NO<sub>x</sub>  
25 emissions: changes in 2005–2012 ship exhaust inferred from satellite measurements over  
26 Europe, *Environ. Res. Lett.*, 10(7), 074007, doi:10.1088/1748-9326/10/7/074007, 2015.

27 Bovensmann, H., Burrows, J. P., Buchwitz, M., Frerick, J., Noël, S., Rozanov, V. V., Chance, K.  
28 V. and Goede, a. P. H.: SCIAMACHY: Mission Objectives and Measurement Modes, *J. Atmos.*  
29 *Sci.*, 56(2), 127–150, doi:10.1175/1520-0469, 1999.

30 Bucsela, E. J., Krotkov, N. A., Celarier, E. A., Lamsal, L. N., Swartz, W. H., Bhartia, P. K.,  
31 Boersma, K. F., Veefkind, J. P., Gleason, J. F. and Pickering, K. E.: A new stratospheric and  
32 tropospheric NO<sub>2</sub> retrieval algorithm for nadir-viewing satellite instruments: applications to  
33 OMI, *Atmos. Meas. Tech.*, 6(1), 2607–2626, doi:10.5194/amt-6-2607-2013, 2013.

34 Burrows, J. P., Buchwitz, M., Rozanov, V., Weber, M., Richter, A., Ladstätter-Weissenmayer, A.  
35 and Eisinger, M.: The Global Ozone Monitoring Experiment (GOME): Mission, instrument  
36 concept, and first scientific results, *Eur. Sp. Agency, (Special Publ. ESA SP, (414 PART 2),*  
37 *585–590*, doi:10.1175/1520-0469, 1997.

38 Burrows, J. P., Weber, M., Buchwitz, M., Rozanov, V. and Ladst, A.: The Global Ozone  
39 Monitoring Experiment ( GOME ): Mission Concept and First Scientific Results Corresponding  
40 Author :, *J. Atmos. Sci.*, 56(2), 151–175, doi:10.1175/1520-0469, 1999.

41 CAAA: EPA History: Clean Air Act Amendments of 1990, [online] Available from:  
42 <http://www2.epa.gov/aboutepa/epa-history-clean-air-act-amendments-1990> (Accessed 7 March

2016), 1990.

CAIR: Programs | Clean Air Markets | US Environmental Protection Agency, [online] Available from: <http://www.epa.gov/airmarkets/programs/> (Accessed 7 March 2016), 2009.

Callies, J., Corpaccioli, E., Eisinger, M., Hahne, A., and Lefebvre, A.: GOME-2 - Metop's second-generation sensor for operational ozone monitoring, ESA Bull. Sp. Agency, 102(may), 28–36, Available from: <http://www.esa.int/esapub/bulletin/bullet102/Callies102.pdf> (Accessed 7 March 2016), 2000.

Carn, S. A., Krueger, A. J., Krotkov, N. A., and Gray, M. A.: Fire at Iraqi sulfur plant emits SO<sub>2</sub> clouds detected by Earth Probe TOMS, Geophys. Res. Lett., 31(19), 2–5, doi:10.1029/2004GL020719, 2004.

Carn, S. A., Krueger, A. J., Krotkov, N. A., Yang, K. and Levelt, P. F.: Sulfur dioxide emissions from Peruvian copper smelters detected by the Ozone Monitoring Instrument, Geophys. Res. Lett., 34(9), doi:10.1029/2006GL029020, 2007.

Castellanos, P. and Boersma, K. F.: Reductions in nitrogen oxides over Europe driven by environmental policy and economic recession., Sci. Rep., 2, 265, doi:10.1038/srep00265, 2012.

Castellanos, P., Marufu, L. T., Doddridge, B. G., Taubman, B. F., Schwab, J. J., Hains, J. C., Ehrman, S. H. and Dickerson, R. R.: Ozone, oxides of nitrogen, and carbon monoxide during pollution events over the eastern United States: An evaluation of emissions and vertical mixing, J. Geophys. Res., 116(D16), D16307, doi:10.1029/2010JD014540, 2011.

Castellanos, P., Boersma, K. F. and van der Werf, G. R.: Satellite observations indicate substantial spatiotemporal variability in biomass burning NO<sub>x</sub> emission factors for South America, Atmos. Chem. Phys., 14(8), 3929–3943, doi:10.5194/acp-14-3929-2014, 2014.

Chance, K., Liu, X., Suleiman, R. M., Flittner, D. E., Al-Saadi, J. and Janz, S. J.: Tropospheric emissions: monitoring of pollution (TEMPO), SPIE Opt. Eng. + Appl., 8866 (Sentinel 4), 88660D, doi:10.1117/12.2024479, 2013.

Chance, K. V. and Spurr, R. J. D.: Ring effect studies: Rayleigh scattering, including molecular parameters for rotational Raman scattering, and the Fraunhofer spectrum, Appl. Opt., 36, 5224–5230, doi:10.1364/AO.36.005224, 1997.

Chubarova, N. Y., Larin, L. K., Lebedev, V. V., Partola, V. S., Lezina, Y. A. and Rublev, A. N.: Experimental and model study of changes in spectral solar irradiance in the atmosphere of large city due to tropospheric NO<sub>2</sub> content, Curren Probl. Atmos. Radiat. (IRS 2008) Ed. by T. Nakajima M.A. Yamasoe, AIP Conf. Proc., 1100(2), 459–462, doi:10.1063/1.3117019, 2009.

Chubarova, N. Y., Poliukhov, A. A. and Gorlova, I. D.: Long-term variability of aerosol optical thickness in Eastern Europe over 2001-2014 according to the measurements at the Moscow MSU MO AERONET site with additional cloud and NO<sub>2</sub> correction, Atmos. Meas. Tech., 9(2), 313–334, doi:10.5194/amt-9-313-2016, 2016.

Curier, R. L., Kranenburg, R., Segers, A. J. S., Timmermans, R. M. A. and Schaap, M.: Synergistic use of OMI NO<sub>2</sub> tropospheric columns and LOTOS–EUROS to evaluate the NO<sub>x</sub> emission trends across Europe, Remote Sens. Environ., 149, 58–69, doi:10.1016/j.rse.2014.03.032, 2014.

Denby, B., Sundvor, I., Cassiani, M., de Smet, P., de Leeuw, F. and Horálek, J.: Spatial mapping of ozone and SO<sub>2</sub> trends in Europe., Sci. Total Environ., 408(20), 4795–806,

doi:10.1016/j.scitotenv.2010.06.021, 2010.

Dickerson, R. R.: Analysis of black carbon and carbon monoxide observed over the Indian Ocean: Implications for emissions and photochemistry, *J. Geophys. Res.*, 107(D19), 8017, doi:10.1029/2001JD000501, 2002.

Dickerson, R. R., Li, C., Li, Z., Marufu, L. T., Stehr, J. W., McClure, B., Krotkov, N., Chen, H., Wang, P., Xia, X., Ban, X., Gong, F., Yuan, J. and Yang, J.: Aircraft observations of dust and pollutants over northeast China: Insight into the meteorological mechanisms of transport, *J. Geophys. Res. Atmos.*, 112(24), 1–13, doi:10.1029/2007JD008999, 2007.

Ding, J., van der A, R. J., Mijling, B., Levelt, P. F. and Hao, N.: NO<sub>x</sub> emission estimates during the 2014 Youth Olympic Games in Nanjing, *Atmos. Chem. Phys.*, 15, 9399–9412,, doi:10.5194/acp-15-9399-2015, 2015.

Dittman, M. G., Ramberg, E., Chrisp, M., Rodriguez, J. V., Sparks, A. L., Zaun, N. H., Hendershot, P., Dixon, T., Philbrick, R. H. and Wasinger, D.: Nadir ultraviolet imaging spectrometer for the NPOESS Ozone Mapping and Profiler Suite (OMPS), *Earth Observing Systems VII*, William L. Barnes, Editor, *Proceedings of SPIE Vol. 4814*, 2002.

Dobber, M. R., Dirksen, R. J., Levelt, P. F., Oord, G. H. J. Van Den, Voors, R. H. M., Kleipool, Q., Jaross, G., Kowalewski, M., Hilsenrath, E., Leppelmeier, G. W., Vries, J. D. V. J. De, Dierssen, W. and Rozemeijer, N. C.: Ozone monitoring instrument calibration, *IEEE Trans. Geosci. Remote Sens.*, 44(5), 1209–1238, doi:10.1109/TGRS.2006.869987, 2006.

Duncan, B. N., Yoshida, Y., Olson, J. R., Sillman, S., Martin, R. V., Lamsal, L., Hu, Y., Pickering, K. E., Retscher, C., Allen, D. J. and Crawford, J. H.: Application of OMI observations to a space-based indicator of NO<sub>x</sub> and VOC controls on surface ozone formation, *Atmos. Environ.*, 44(18), 2213–2223, doi:10.1016/j.atmosenv.2010.03.010, 2010.

Duncan, B. N., Yoshida, Y., de Foy, B., Lamsal, L. N., Streets, D. G., Lu, Z., Pickering, K. E. and Krotkov, N. A.: The observed response of Ozone Monitoring Instrument (OMI) NO<sub>2</sub> columns to NO<sub>x</sub> emission controls on power plants in the United States: 2005–2011, *Atmos. Environ.*, 81, 102–111, doi:10.1016/j.atmosenv.2013.08.068, 2013.

Duncan, B. N., Prados, A. I., Lamsal, L. N., Liu, Y., Streets, D. G., Gupta, P., Hilsenrath, E., Kahn, R. A., Nielsen, J. E., Beyersdorf, A. J., Burton, S. P., Fiore, A. M., Fishman, J., Henze, D. K., Hostetler, C. A., Krotkov, N. A., Lee, P., Lin, M., Pawson, S., Pfister, G., Pickering, K. E., Pierce, R. B., Yoshida, Y. and Ziemba, L. D.: Satellite data of atmospheric pollution for U.S. air quality applications: Examples of applications, summary of data end-user resources, answers to FAQs, and common mistakes to avoid, *Atmos. Environ.*, 94, 647–662, doi:10.1016/j.atmosenv.2014.05.061, 2014.

Duncan, B. N., Lamsal, L. N., Thompson, A. M., Yoshida, Y., Lu, Z., Streets, D. G., Hurwitz, M. M. and Pickering, K. E.: A space-based, high-resolution view of notable changes in urban NO<sub>x</sub> pollution around the world (2005–2014), *J. Geophys. Res. Atmos.*, 121(2), 976–996, doi:10.1002/2015JD024121, 2016.

EEA: European Union emission inventory report 1990–2011 under the UNECE Convention on Long-range Transboundary Air Pollution (LRTAP), European Environment Agency (EEA), Technical report No 10/2013, doi:10.2800/44480, 2013.

Eisinger, M. and Burrows, J. P.: Tropospheric sulfur dioxide observed by the ERS-2 GOME

1 instrument, *Geophys. Res. Lett.*, 25(22), 4177–4180, doi:10.1029/1998GL900128, 1998.

2 Elansky, N. F., Lokoshchenko, M. a., Belikov, I. B., Skorokhod, a. I. and Shumskii, R. a.:  
3 Variability of trace gases in the atmospheric surface layer from observations in the city of  
4 Moscow, *Izv. Atmos. Ocean. Phys.*, 43(2), 219–231, doi:10.1134/S0001433807020089, 2007.

5 EPA: Reactive Nitrogen in the United States: An Analysis of Inputs, Flows, Consequences, and  
6 Management Options, Washington, DC. [online] Available from:  
7 [http://yosemite.epa.gov/sab/sabproduct.nsf/WebBOARD/INCFullReport/\\$File/Final INC](http://yosemite.epa.gov/sab/sabproduct.nsf/WebBOARD/INCFullReport/$File/Final%20Report_8_19_11(without%20signatures).pdf)  
8 [Report\\_8\\_19\\_11\(without signatures\).pdf](http://yosemite.epa.gov/sab/sabproduct.nsf/WebBOARD/INCFullReport/$File/Final INC Report_8_19_11(without signatures).pdf) (Accessed 7 March 2016), 2011.

9 EPA: Integrated Science Assessment of Ozone and Related Photochemical Oxidants, [online]  
10 Available from: <http://cfpub.epa.gov/ncea/isa/recordisplay.cfm?deid=247492#Download>  
11 (Accessed 7 March 2016), 2013.

12 European Commission: Air Quality Standards - Environment - European Commission, [online]  
13 Available from: <http://ec.europa.eu/environment/air/quality/standards.htm> (Accessed 7 March  
14 2017), 2015.

15 Fioletov, V., McLinden, C., Krotkov, N. A. and Li, C.: A global catalogue of SO<sub>2</sub> sources and  
16 emissions derived from Ozone Monitoring Instrument, prepared for *Atmos. Chem. Phys.*, 2016.

17 Fioletov, V. E., McLinden, C. A., Krotkov, N., Moran, M. D. and Yang, K.: Estimation of SO<sub>2</sub>  
18 emissions using OMI retrievals, *Geophys. Res. Lett.*, 38(21), doi:10.1029/2011GL049402, 2011.

19 Fioletov, V. E., McLinden, C. a., Krotkov, N., Yang, K., Loyola, D. G., Valks, P., Theys, N.,  
20 Van Roozendaal, M., Nowlan, C. R., Chance, K., Liu, X., Lee, C. and Martin, R. V.: Application  
21 of OMI, SCIAMACHY, and GOME-2 satellite SO<sub>2</sub> retrievals for detection of large emission  
22 sources, *J. Geophys. Res. Atmos.*, 118(19), 11399–11418, doi:10.1002/jgrd.50826, 2013.

23 Fioletov, V. E., McLinden, C. A., Krotkov, N. and Li, C.: Lifetimes and emissions of SO<sub>2</sub> from  
24 point sources estimated from OMI, *Geophys. Res. Lett.*, 42(6), 1969–1976,  
25 doi:10.1002/2015GL063148, 2015.

26 Flynn, L., Long, C., Wu, X., Evans, R., Beck, C. T., Petropavlovskikh, I., McConville, G., Yu,  
27 W., Zhang, Z., Niu, J., Beach, E., Hao, Y., Pan, C., Sen, B., Novicki, M., Zhou, S. and Seftor, C.:  
28 Performance of the Ozone Mapping and Profiler Suite (OMPS) products, *J. Geophys. Res.*  
29 *Atmos.*, 119(10), 6181–6195, doi:10.1002/2013JD020467, 2014.

30 de Foy, B., Krotkov, N. A., Bei, N., Herndon, S. C., Huey, L. G., Martínez, A.-P., Ruiz-Suárez,  
31 L. G., Wood, E. C., Zavala, M. and Molina, L. T.: Hit from both sides: tracking industrial and  
32 volcanic plumes in Mexico City with surface measurements and OMI SO<sub>2</sub> retrievals during the  
33 MILAGRO field campaign, *Atmos. Chem. Phys.*, 9(24), 9599–9617, doi:10.5194/acp-9-9599-  
34 2009, 2009.

35 de Foy, B., Wilkins, J. L., Lu, Z., Streets, D. G. and Duncan, B. N.: Model evaluation of methods  
36 for estimating surface emissions and chemical lifetimes from satellite data, *Atmos. Environ.*, 98,  
37 66–77, doi:10.1016/j.atmosenv.2014.08.051, 2014.

38 de Foy, B., Lu, Z., Streets, D. G., Lamsal, L. N. and Duncan, B. N.: Estimates of power plant  
39 NO<sub>x</sub> emissions and lifetimes from OMI NO<sub>2</sub> satellite retrievals, *Atmos. Environ.*, 116, 1–11,  
40 doi:10.1016/j.atmosenv.2015.05.056, 2015.

41 Frost, G. J., McKeen, S. A., Trainer, M., Ryerson, T. B., Neuman, J. A., Roberts, J. M.,  
42 Swanson, A., Holloway, J. S., Sueper, D. T., Fortin, T., Parrish, D. D., Fehsenfeld, F. C., Flocke,

1 F., Peckham, S. E., Grell, G. A., Kowal, D., Cartwright, J., Auerbach, N. and Habermann, T.:  
2 Effects of changing power plant NO<sub>x</sub> emissions on ozone in the eastern United States: Proof of  
3 concept, *J. Geophys. Res.*, 111(D12), D12306, doi:10.1029/2005JD006354, 2006.

4 Galloway, J. N., Leach, A. M., Bleeker, A. and Erisman, J. W.: A chronology of human  
5 understanding of the nitrogen cycle, *Philos. Trans. R. Soc. London B Biol. Sci.*, 368(1621)  
6 [online] Available from:  
7 <http://rstb.royalsocietypublishing.org/content/368/1621/20130120.abstract> , 2013.

8 Geddes, J. A., Murphy, J. G., O'Brien, J. M. and Celarier, E. A.: Biases in long-term NO<sub>2</sub>  
9 averages inferred from satellite observations due to cloud selection criteria, *Remote Sens.*  
10 *Environ.*, 124, 210–216, doi:10.1016/j.rse.2012.05.008, 2012.

11 Ghude, S. D., Lal, D. M., Beig, G., Van Der A, R. and Sable, D.: Rain-induced soil NO<sub>x</sub>  
12 emission from India during the onset of the summer monsoon: A satellite perspective, *J.*  
13 *Geophys. Res. Atmos.*, 115(16), doi:10.1029/2009JD013367, 2010.

14 Ghude, S. D., Kulkarni, P. S., Kulkarni, S. H., Fadnavis, S. and Van Der A, R. J.: Temporal  
15 variation of urban NO<sub>x</sub> concentration in India during the past decade as observed from space,  
16 *Int. J. Remote Sens.*, 32(3), 849–861, doi:10.1080/01431161.2010.517797, 2011.

17 Ghude, S. D., Pfister, G. G., Jena, C., Van Der A, R. J., Emmons, L. K. and Kumar, R.: Satellite  
18 constraints of nitrogen oxide (NO<sub>x</sub>) emissions from India based on OMI observations and WRF-  
19 Chem simulations, *Geophys. Res. Lett.*, 40(2), 423–428, doi:10.1029/2012GL053926, 2013.

20 Gorchakov, G., Semoutnikova, E., Karpov, A., and Lezina, E.: Air Pollution in Moscow  
21 Megacity, Chapter 11, in: *Advanced Topics in Environmental Health and Air Pollution Case*  
22 *Studies*, edited by Moldoveanu, A. M., InTech., 2011.

23 Guay, J.: China's Thirst for Coal Is Drying Up, [online] Available from:  
24 [http://www.huffingtonpost.com/justin-guay/chinas-thirst-for-coal-is\\_b\\_5358194.html](http://www.huffingtonpost.com/justin-guay/chinas-thirst-for-coal-is_b_5358194.html) (Accessed  
25 7 March 2016), 2015.

26 Hand, J. L., Schichtel, B. A., Malm, W. C. and Pitchford, M. L.: Particulate sulfate ion  
27 concentration and SO<sub>2</sub> emission trends in the United States from the early 1990s through 2010,  
28 *Atmos. Chem. Phys.*, 12(21), 10353–10365, doi:10.5194/acp-12-10353-2012, 2012.

29 Hayn, M., Beirle, S., Hamprecht, F. A., Platt, U., Menze, B. H. and Wagner, T.: Analysing  
30 spatio-temporal patterns of the global NO<sub>2</sub>-distribution retrieved from GOME satellite  
31 observations using a generalized additive model, *Atmos. Chem. Phys.*, 9(17), 6459–6477,  
32 doi:10.5194/acp-9-6459-2009, 2009.

33 He, H., Li, C., Loughner, C. P., Li, Z., Krotkov, N. A., Yang, K., Wang, L., Zheng, Y., Bao, X.,  
34 Zhao, G. and Dickerson, R. R.: SO<sub>2</sub> over central China : Measurements, numerical simulations  
35 and the tropospheric sulfur budget, , 117, 1–15, doi:10.1029/2011JD016473, 2012.

36 He, H., Vinnikov, K., Li, C., Krotkov, N. A., Jongeward, A. R., Li, Z., Stehr, J. W., Hains, J. C.  
37 and Dickerson, R. R.: Response of SO<sub>2</sub> and particulate air pollution to local and regional  
38 emission controls: A case study in Maryland, under review, *Earth's Future*, 2016.

39 Herman, J., Deland, M. T., Huang, L. K., Labow, G., Larko, D., Lloyd, S. A., Mao, J., Qin, W.  
40 and Weaver, C.: A net decrease in the Earth's cloud, aerosol, and surface 340 nm reflectivity  
41 during the past 33 yr (1979–2011), *Atmos. Chem. Phys.*, 13(16), 8505–8524, doi:10.5194/acp-  
42 13-8505-2013, 2013.



1 Hilboll, A., Richter, A. and Burrows, J. P.: Long-term changes of tropospheric NO<sub>2</sub> over  
2 megacities derived from multiple satellite instruments, *Atmos. Chem. Phys.*, 13(8), 4145–4169,  
3 doi:10.5194/acp-13-4145-2013, 2013.

4 Hogrefe, C., Hao, W., Zalewsky, E. E., Ku, J.-Y., Lynn, B., Rosenzweig, C., Schultz, M. G.,  
5 Rast, S., Newchurch, M. J., Wang, L., Kinney, P. L. and Sistla, G.: An analysis of long-term  
6 regional-scale ozone simulations over the Northeastern United States: variability and trends,  
7 *Atmos. Chem. Phys.*, 11(2), 567–582, doi:10.5194/acp-11-567-2011, 2011.

8 Huang, J., Zhou, C., Lee, X., Bao, Y., Zhao, X., Fung, J., Richter, A., Liu, X. and Zheng, Y.: The  
9 effects of rapid urbanization on the levels in tropospheric nitrogen dioxide and ozone over East  
10 China, *Atmos. Environ.*, 77, 558–567, doi:10.1016/j.atmosenv.2013.05.030, 2013.

11 Ialongo, I., Hakkarainen, J., Kivi, R., Anttila, P., Krotkov, N. A., Yang, K., Li, C., Tukiainen, S.,  
12 Hassinen, S. and Tamminen, J.: Comparison of operational satellite SO<sub>2</sub> products with ground-  
13 based observations in northern Finland during the Icelandic Holuhraun fissure eruption, *Atmos.*  
14 *Meas. Tech.*, 8(6), 2279–2289, doi:10.5194/amt-8-2279-2015, 2015.

15 Ingmann, P., Veihelmann, B., Langen, J., Lamarre, D., Stark, H. and Courrèges-Lacoste, G. B.:  
16 Requirements for the GMES Atmosphere Service and ESA's implementation concept: Sentinels-  
17 4/-5 and -5p, *Remote Sens. Environ.*, 120, 58–69, doi:10.1016/j.rse.2012.01.023, 2012.

18 IPCC Working Group I, I., Stocker, T. F., Qin, D., Plattner, G.-K., Tignor, M., Allen, S. K.,  
19 Boschung, J., Nauels, A., Xia, Y., Bex, V. and Midgley, P. M.: IPCC, 2013: Climate Change  
20 2013: The Physical Science Basis. Contribution of Working Group I to the Fifth Assessment  
21 Report of the Intergovernmental Panel on Climate Change, IPCC, AR5, 1535, 2013.

22 Irie, H., Boersma, K. F., Kanaya, Y., Takashima, H., Pan, X. and Wang, Z. F.: Quantitative bias  
23 estimates for tropospheric NO<sub>2</sub> columns retrieved from SCIAMACHY, OMI, and GOME-2  
24 using a common standard for East Asia, *Atmos. Meas. Tech.*, 5(10), 2403–2411,  
25 doi:10.5194/amt-5-2403-2012, 2012.

26 Janssens-Maenhout, G., Crippa, M., Guizzardi, D., Dentener, F., Muntean, M., Pouliot, G.,  
27 Keating, T., Zhang, Q., Kurokawa, J., Wankmüller, R., Denier van der Gon, H., Kuenen, J. J. P.,  
28 Klimont, Z., Frost, G., Darras, S., Koffi, B. and Li, M.: HTAP\_v2.2: a mosaic of regional and  
29 global emission grid maps for 2008 and 2010 to study hemispheric transport of air pollution,  
30 *Atmos. Chem. Phys.*, 15(19), 11411–11432, doi:10.5194/acp-15-11411-2015, 2015.

31 Jia, B., Wang, Y., Yao, Y. and Xie, Y.: A new indicator on the impact of large-scale circulation  
32 on wintertime particulate matter pollution over China, *Atmos. Chem. Phys.*, 15, 11919–11929,  
33 doi:10.5194/acp-15-11919-2015, 2015.

34 Khokhar, M. F., Frankenberg, C., Van Roozendaal, M., Beirle, S., Köhl, S., Richter, A., Platt, U.  
35 and Wagner, T.: Satellite observations of atmospheric SO<sub>2</sub> from volcanic eruptions during the  
36 time-period of 1996–2002, in *Advances in Space Research*, vol. 36, pp. 879–887., 2005.

37 Kim, J.: GEMS(Geostationary Environment Monitoring Spectrometer) onboard the  
38 GeoKOMPSAT to Monitor Air Quality in high Temporal and Spatial Resolution over Asia-  
39 Pacific Region, EGU Gen. Assem. 2012 [online] Available from:  
40 <http://adsabs.harvard.edu/abs/2012EGUGA..14.4051K> (Accessed 7 March 2016), 2012.

41 Kim, S. W., Heckel, A., Frost, G. J., Richter, A., Gleason, J., Burrows, J. P., McKeen, S., Hsie,  
42 E. Y., Granier, C. and Trainer, M.: NO<sub>2</sub> columns in the western United States observed from



space and simulated by a regional chemistry model and their implications for NO<sub>x</sub> emissions, *J. Geophys. Res. Atmos.*, 114(11), doi:10.1029/2008JD011343, 2009.

Klimont, Z., Cofala, J., Xing, J., Wei, W., Zhang, C., Wang, S., Kejun, J., Bhandari, P., Mathur, R., Purohit, P., Rafaj, P., Chambers, A., Amann, M. and Hao, J.: Projections of SO<sub>2</sub>, NO<sub>x</sub> and carbonaceous aerosols emissions in Asia, *Tellus B*, 61(4), doi:10.3402/tellusb.v61i4.16858, 2009.

Klimont, Z., Smith, S. J. and Cofala, J.: The last decade of global anthropogenic sulfur dioxide: 2000–2011 emissions, *Environ. Res. Lett.*, 8(1), 014003, doi:10.1088/1748-9326/8/1/014003, 2013.

KNMI: Background information about the Row Anomaly in OMI, [online] Available from: <http://www.knmi.nl/omi/research/product/rowanomaly-background.php> (Accessed 7 March 2016), 2012.

Kononov, I. B., Beekmann, M., Richter, A. and Burrows, J. P.: Inverse modelling of the spatial distribution of NO<sub>x</sub> emissions on a continental scale using satellite data, *Atmos. Chem. Phys.*, 6(7), 1747–1770, doi:10.5194/acp-6-1747-2006, 2006.

Kononov, I. B., Beekmann, M., Richter, A., Burrows, J. P. and Hilboll, A.: Multi-annual changes of NO<sub>x</sub> emissions in megacity regions: Nonlinear trend analysis of satellite measurement based estimates, *Atmos. Chem. Phys.*, 10(17), 8481–8498, doi:10.5194/acp-10-8481-2010, 2010.

Krotkov, N. A., Cam, S. A., Krueger, A. J., Bhartia, P. K. and Yang, K.: Band residual difference algorithm for retrieval of SO<sub>2</sub> from the Aura Ozone Monitoring Instrument (OMI), *IEEE Trans. Geosci. Remote Sens.*, 44(5), 1259–1266, doi:10.1109/TGRS.2005.861932, 2006.

Krotkov, N. A., McClure, B., Dickerson, R. R., Carn, S. A., Li, C., Bhartia, P. K., Yang, K., Krueger, A. J., Li, Z., Levelt, P. F., Chen, H., Wang, P. and Lu, D.: Validation of SO<sub>2</sub> retrievals from the Ozone Monitoring Instrument over NE China, *J. Geophys. Res. Atmos.*, 113(16), doi:10.1029/2007JD008818, 2008.

Krueger, A. J.: Sighting of El Chichon sulfur dioxide clouds with the Nimbus 7 total ozone mapping spectrometer, *Science*, 220(4604), 1377–9, doi:10.1126/science.220.4604.1377, 1983.

Lamsal, L. N., Martin, R. V., van Donkelaar, A., Steinbacher, M., Celarier, E. A., Bucsela, E., Dunlea, E. J. and Pinto, J. P.: Ground-level nitrogen dioxide concentrations inferred from the satellite-borne Ozone Monitoring Instrument, *J. Geophys. Res. Atmos.*, 113(16), doi:10.1029/2007JD009235, 2008.

Lamsal, L. N., Martin, R. V., Van Donkelaar, A., Celarier, E. A., Bucsela, E. J., Boersma, K. F., Dirksen, R., Luo, C. and Wang, Y.: Indirect validation of tropospheric nitrogen dioxide retrieved from the OMI satellite instrument: Insight into the seasonal variation of nitrogen oxides at northern midlatitudes, *J. Geophys. Res. Atmos.*, 115(5), doi:10.1029/2009JD013351, 2010.

Lamsal, L. N., Martin, R. V., Padmanabhan, A., van Donkelaar, A., Zhang, Q., Sioris, C. E., Chance, K., Kurosu, T. P. and Newchurch, M. J.: Application of satellite observations for timely updates to global anthropogenic NO<sub>x</sub> emission inventories, *Geophys. Res. Lett.*, 38(5), n/a–n/a, doi:10.1029/2010GL046476, 2011.

Lamsal, L. N., Martin, R. V., Parrish, D. D. and Krotkov, N. A.: Scaling relationship for NO<sub>2</sub> pollution and urban population size: A satellite perspective, *Environ. Sci. Technol.*, 47(14),

1 7855–7861, doi:10.1021/es400744g, 2013.

2 Lamsal, L. N., Duncan, B. N., Yoshida, Y., Krotkov, N. A., Pickering, K. E., Streets, D. G. and  
3 Lu, Z.: U.S. NO<sub>2</sub> trends (2005–2013): EPA Air Quality System (AQS) data versus improved  
4 observations from the Ozone Monitoring Instrument (OMI), *Atmos. Environ.*, 110, 130–143,  
5 doi:10.1016/j.atmosenv.2015.03.055, 2015.

6 Lee, C., Martin, R. V., Van Donkelaar, A., O’Byrne, G., Krotkov, N., Richter, A., Huey, L. G.  
7 and Holloway, J. S.: Retrieval of vertical columns of sulfur dioxide from SCIAMACHY and  
8 OMI: Air mass factor algorithm development, validation, and error analysis, *J. Geophys. Res.*  
9 *Atmos.*, 114(22), doi:10.1029/2009JD012123, 2009.

10 Lee, C., Martin, R. V., Van Donkelaar, A., Lee, H., Dickerson, R. R., Hains, J. C., Krotkov, N.,  
11 Richter, A., Vinnikov, K. and Schwab, J. J.: SO<sub>2</sub> emissions and lifetimes: Estimates from inverse  
12 modeling using in situ and global, space-based (SCIAMACHY and OMI) observations, *J.*  
13 *Geophys. Res. Atmos.*, 116(6), doi:10.1029/2010JD014758, 2011.

14 Lee, C. J., Martin, R. V., Henze, D. K., Brauer, M., Cohen, A. and Donkelaar, A. Van: Response  
15 of Global Particulate-Matter-Related Mortality to Changes in Local Precursor Emissions,  
16 *Environ. Sci. Technol.*, 150324080130001, doi:10.1021/acs.est.5b00873, 2015.

17 Lelieveld, J., Beirle, S., Hörmann, C., Stenchikov, G. and Wagner, T.: Abrupt recent trend  
18 changes in atmospheric nitrogen dioxide over the Middle East, *Sci. Adv.*, 1(7), 2–6, 2015.

19 Leue, C., Wenig, M., Wagner, T., Klimm, O., Platt, U. and Jähne, B.: Quantitative analysis of  
20 NO<sub>x</sub> emissions from Global Ozone Monitoring Experiment satellite image sequences, *J.*  
21 *Geophys. Res.*, 106(D6), 5493, doi:10.1029/2000JD900572, 2001.

22 Levelt, P. F., Hilsenrath, E., Leppelmeier, G. W., Oord, G. H. J. Van Den, Bhartia, P. K.,  
23 Tamminen, J., Haan, J. F. De and Veeffkind, J. P.: Science Objectives of the Ozone Monitoring  
24 Instrument, *IEEE Trans. Geosci. Remote Sens.*, 44(5), 1199–1208, 2006a.

25 Levelt, P. F., Oord, G. H. J. Van Den, Dobber, M. R., Mälkki, A., Visser, H., Vries, J. De,  
26 Stammes, P., Lundell, J. O. V and Saari, H.: The Ozone Monitoring Instrument, *IEEE Trans.*  
27 *Geosci. Remote Sens.*, 44(5), 1093–1101, 2006b.

28 Li, C., Marufu, L. T., Dickerson, R. R., Li, Z., Wen, T., Wang, Y., Wang, P., Chen, H. and Stehr,  
29 J. W.: In situ measurements of trace gases and aerosol optical properties at a rural site in northern  
30 China during East Asian Study of Tropospheric Aerosols: An International Regional Experiment  
31 2005, *J. Geophys. Res.*, 112(D22), D22S04, doi:10.1029/2006JD007592, 2007.

32 Li, C., Zhang, Q., Krotkov, N. A., Streets, D. G., He, K., Tsay, S.-C. and Gleason, J. F.: Recent  
33 Large Reduction in Sulfur Dioxide Emissions from Chinese Power Plants Observed by the  
34 Ozone Monitoring Instrument, *Geophys. Res. Lett.*, 37, 1–6, doi:10.1029/2010GL042594, 2010.

35 Li, C., Joiner, J., Krotkov, N. a. and Bhartia, P. K.: A fast and sensitive new satellite SO<sub>2</sub>  
36 retrieval algorithm based on principal component analysis: Application to the ozone monitoring  
37 instrument, *Geophys. Res. Lett.*, 40(23), 6314–6318, doi:10.1002/2013GL058134, 2013.

38 Liu, Y., Chen, X., Huang, S., Tian, L., Lu, Y., Mei, Y., Ren, M., Li, N., Liu, L. and Xiang, H.:  
39 Association between air pollutants and cardiovascular disease mortality in Wuhan, China., *Int. J.*  
40 *Environ. Res. Public Health*, 12(4), 3506–16, doi:10.3390/ijerph120403506, 2015.

41 Lookman, A. A. and Rubin, E. S.: Barriers to adopting least-cost particulate control strategies for  
42 Indian power plants, *Energy Policy*, 26(14), 1053–1063, doi:10.1016/S0301-4215(98)00049-4,

1998.

Lu, Z. and Streets, D. G.: Increase in NO<sub>x</sub> emissions from Indian thermal power plants during 1996-2010: unit-based inventories and multisatellite observations., *Environ. Sci. Technol.*, 46(14), 7463–70, doi:10.1021/es300831w, 2012.

Lu, Z., Streets, D. G., Zhang, Q., Wang, S., Carmichael, G. R., Cheng, Y. F., Wei, C., Chin, M., Diehl, T. and Tan, Q.: Sulfur dioxide emissions in China and sulfur trends in East Asia since 2000, *Atmos. Chem. Phys.*, 10(13), 6311–6331, doi:10.5194/acp-10-6311-2010, 2010.

Lu, Z., Zhang, Q. and Streets, D. G.: Sulfur dioxide and primary carbonaceous aerosol emissions in China and India, 1996–2010, *Atmos. Chem. Phys.*, 11(18), 9839–9864, doi:10.5194/acp-11-9839-2011, 2011.

Lu, Z., Streets, D. G., De Foy, B. and Krotkov, N. A.: Ozone monitoring instrument observations of interannual increases in SO<sub>2</sub> emissions from Indian coal-fired power plants during 2005-2012, *Environ. Sci. Technol.*, 47(24), 13993–14000, doi:10.1021/es4039648, 2013.

Lu, Z., Streets, D. G., de Foy, B., Lamsal, L. N., Duncan, B. N. and Xing, J.: Emissions of nitrogen oxides from US urban areas: estimation from Ozone Monitoring Instrument retrievals for 2005–2014, *Atmos. Chem. Phys.*, 15(18), 10367–10383, doi:10.5194/acp-15-10367-2015, 2015.

Martin, R. V.: Satellite remote sensing of surface air quality, *Atmos. Environ.*, 42(34), 7823–7843, doi:10.1016/j.atmosenv.2008.07.018, 2008.

Martin, R. V., Chance, K., Jacob, D. J., Kurosu, T. P., Spurr, R. J. D., Bucsela, E., Gleason, J. F., Palmer, P. I., Bey, I., Fiore, A. M., Li, Q., Yantosca, R. M. and Koelemeijer, R. B. A.: An improved retrieval of tropospheric nitrogen dioxide from GOME, *J. Geophys. Res.*, 107(20), 4437, doi:10.1029/2001JD001027, 2002.

McLinden, C. A., Fioletov, V., Boersma, K. F., Krotkov, N., Sioris, C. E., Veefkind, J. P. and Yang, K.: Air quality over the Canadian oil sands: A first assessment using satellite observations, *Geophys. Res. Lett.*, 39(4), doi:10.1029/2011GL050273, 2012.

McLinden, C. A., Fioletov, V., Boersma, K. F., Kharol, S. K., Krotkov, N., Lamsal, L., Makar, P. A., Martin, R. V., Veefkind, J. P. and Yang, K.: Improved satellite retrievals of NO<sub>2</sub> and SO<sub>2</sub> over the Canadian oil sands and comparisons with surface measurements, *Atmos. Chem. Phys.*, 14(7), 3637–3656, doi:10.5194/acp-14-3637-2014, 2014.

McLinden, C. A., Fioletov, V., Krotkov, N. A., Li, C., Boersma, K. F. and Adams, C.: A Decade of Change in NO<sub>2</sub> and SO<sub>2</sub> over the Canadian Oil Sands As Seen from Space., *Environ. Sci. Technol.*, 50(1), 331–7, doi:10.1021/acs.est.5b04985, 2016.

Mebust, A. K. and Cohen, R. C.: Space-based observations of fire NO<sub>x</sub> emission coefficients: a global biome-scale comparison, *Atmos. Chem. Phys.*, 14(5), 2509–2524, doi:10.5194/acp-14-2509-2014, 2014.

MEP: The airborne pollution prevention and control action plan, [online] Available from: [http://english.mep.gov.cn/News\\_service/infocus/201309/t20130924\\_260707.htm](http://english.mep.gov.cn/News_service/infocus/201309/t20130924_260707.htm) (Accessed 7 March 2016), 2013.

Mijling, B. and Van Der A, R. J.: Using daily satellite observations to estimate emissions of short-lived air pollutants on a mesoscopic scale, *J. Geophys. Res. Atmos.*, 117(17), 1–20, doi:10.1029/2012JD017817, 2012.

1 Mijling, B., van der A, R. J., Boersma, K. F., Van Roozendaal, M., De Smedt, I. and Kelder, H.  
2 M.: Reductions of NO<sub>2</sub> detected from space during the 2008 Beijing Olympic Games, *Geophys.*  
3 *Res. Lett.*, 36(13), L13801, doi:10.1029/2009GL038943, 2009.

4 Miyazaki, K., Eskes, H. J. and Sudo, K.: Global NO<sub>x</sub> emission estimates derived from an  
5 assimilation of OMI tropospheric NO<sub>2</sub> columns, *Atmos. Chem. Phys.*, 12(5), 2263–2288,  
6 doi:10.5194/acp-12-2263-2012, 2012.

7 Napelenok, S. L., Pinder, R. W., Gilliland, A. B. and Martin, R. V.: A method for evaluating  
8 spatially-resolved NO<sub>x</sub> emissions using Kalman filter inversion, direct sensitivities, and space-  
9 based NO<sub>2</sub> observations, *Atmos. Chem. Phys.*, 8(18), 5603–5614, doi:10.5194/acp-8-5603-2008,  
10 2008.

11 Nowlan, C. R., Martin, R. V., Philip, S., Lamsal, L. N., Krotkov, N. A., Marais, E. A., Wang, S.  
12 and Zhang, Q.: Global dry deposition of nitrogen dioxide and sulfur dioxide inferred from space-  
13 based measurements, *Global Biogeochem. Cycles*, 28(10), 1025–1043,  
14 doi:10.1002/2014GB004805, 2014.

15 Oetjen, H., Baidar, S., Krotkov, N. a., Lamsal, L. N., Lechner, M. and Volkamer, R.: Airborne  
16 MAX-DOAS measurements over California: Testing the NASA OMI tropospheric NO<sub>2</sub> product,  
17 *J. Geophys. Res. Atmos.*, 118(13), 7400–7413, doi:10.1002/jgrd.50550, 2013.

18 Pourzamani, H., Aliyan, T. and Daryalal, M.: Evaluation of SO<sub>2</sub> level in the ambient air of  
19 Khark Island, *Int. J. Environ. Health Eng.*, 1(1), 39, doi:10.4103/2277-9183.102368, 2012.

20 Reuter, M., Buchwitz, M., Hilboll, A., Richter, A., Schneising, O., Hilker, M., Heymann, J.,  
21 Bovensmann, H. and Burrows, J. P.: Decreasing emissions of NO<sub>x</sub> relative to CO<sub>2</sub> in East Asia  
22 inferred from satellite observations, *Nat. Geosci.*, 7(11), 792–795, doi:10.1038/ngeo2257, 2014.

23 Richter, A. and Burrows, J. P.: Tropospheric NO<sub>2</sub> from GOME measurements, *Adv. Sp. Res.*,  
24 2(2), 1–11, 2002.

25 Richter, A., Burrows, J. P., Nüss, H., Granier, C. and Niemeier, U.: Increase in tropospheric  
26 nitrogen dioxide over China observed from space., *Nature*, 437(7055), 129–132,  
27 doi:10.1038/nature04092, 2005.

28 Richter, A., Begoin, M., Hilboll, A. and Burrows, J. P.: An improved NO<sub>2</sub> retrieval for the  
29 GOME-2 satellite instrument, *Atmos. Meas. Tech.*, 4(6), 1147–1159, doi:10.5194/amt-4-1147-  
30 2011, 2011.

31 Richter, A., Hillbol, A. and Burrows, J. P.: Improving S5P NO<sub>2</sub> retrievals, [online] Available  
32 from: [http://seom.esa.int/atmos2015/page\\_presentations.php](http://seom.esa.int/atmos2015/page_presentations.php) (Accessed 7 March 2016), 2015.

33 Rix, M., Valks, P., Hao, N., Loyola, D., Schlager, H., Huntrieser, H., Flemming, J., Koehler, U.,  
34 Schumann, U. and Inness, A.: Volcanic SO<sub>2</sub>, BrO and plume height estimations using GOME-2  
35 satellite measurements during the eruption of Eyjafjallajökull in May 2010, *J. Geophys. Res.*  
36 *Atmos.*, 117(6), doi:10.1029/2011JD016718, 2012.

37 Russell, A. R., Valin, L. C. and Cohen, R. C.: Trends in OMI NO<sub>2</sub> observations over the United  
38 States: effects of emission control technology and the economic recession, *Atmos. Chem. Phys.*,  
39 12(24), 12197–12209, doi:10.5194/acp-12-12197-2012, 2012.

40 Schmidt, A., Leadbetter, S., Theys, N., Carboni, E., Witham, C. S., Stevenson, J. A., Birch, C.  
41 E., Thordarson, T., Turnock, S., Barsotti, S., Delaney, L., Feng, W., Grainger, R. G., Hort, M. C.,  
42 Höskuldsson, Á., Ialongo, I., Ilyinskaya, E., Jóhannsson, T., Kenny, P., Mather, T. A., Richards,

1 N. A. D. and Shepherd, J.: Satellite detection, long-range transport, and air quality impacts of  
2 volcanic sulfur dioxide from the 2014-2015 flood lava eruption at Bárðarbunga (Iceland), J.  
3 Geophys. Res. Atmos., 120(18), 9739–9757, doi:10.1002/2015JD023638, 2015.

4 Schneider, P. and Van Der A, R. J.: A global single-sensor analysis of 2002-2011 tropospheric  
5 nitrogen dioxide trends observed from space, J. Geophys. Res. Atmos., 117(16),  
6 doi:10.1029/2012JD017571, 2012.

7 Schneider, P., Lahoz, W. A. and van der A, R.: Recent satellite-based trends of tropospheric  
8 nitrogen dioxide over large urban agglomerations worldwide, Atmos. Chem. Phys., 15(3), 1205–  
9 1220, doi:10.5194/acp-15-1205-2015, 2015.

10 Schoeberl, M. R., Douglass, A. R., Hilsenrath, E., Bhartia, P. K., Beer, R., Waters, J. W.,  
11 Gunson, M. R., Froidevaux, L., Gille, J. C., Barnett, J. J., Levelt, P. F. and DeCola, P.: Overview  
12 of the EOS aura mission, IEEE Trans. Geosci. Remote Sens., 44(5), 1066–1072,  
13 doi:10.1109/TGRS.2005.861950, 2006.

14 Schumann, U. and Huntrieser, H.: The global lightning-induced nitrogen oxides source, Atmos.  
15 Chem. Phys., 7(14), 3823–3907, doi:10.5194/acp-7-3823-2007, 2007.

16 Seftor, C. J., Jaross, G., Kowitt, M., Haken, M., Li, J. and Flynn, L. E.: Postlaunch performance  
17 of the Suomi National Polar-orbiting Partnership Ozone Mapping and Profiler Suite (OMPS)  
18 nadir sensors, J. Geophys. Res. Atmos., 119(7), 4413–4428, doi:10.1002/2013JD020472, 2014.

19 Seinfeld, J. H. and Pandis, S. N.: Atmospheric Chemistry and Physics: From Air Pollution to  
20 Climate Change, 2nd Edn. 2006, John Wiley & Sons, Hoboken, New Jersey, 2006.

21 Simon, H., Reff, A., Wells, B., Xing, J. and Frank, N.: Ozone trends across the United States  
22 over a period of decreasing NO<sub>x</sub> and VOC emissions., Environ. Sci. Technol., 49(1), 186–95,  
23 doi:10.1021/es504514z, 2015.

24 Smith, S. J., van Aardenne, J., Klimont, Z., Andres, R. J., Volke, A. and Delgado Arias, S.:  
25 Anthropogenic sulfur dioxide emissions: 1850–2005, Atmos. Chem. Phys., 11(3), 1101–1116,  
26 doi:10.5194/acp-11-1101-2011, 2011.

27 Solomon, P. A., Crumpler, D., Flanagan, J. B., Jayanty, R. K. M., Rickman, E. E. and McDade,  
28 C. E.: U.S. national PM<sub>2.5</sub> Chemical Speciation Monitoring Networks-CSN and IMPROVE:  
29 description of networks., J. Air Waste Manag. Assoc., 64(12), 1410–38 [online] Available from:  
30 <http://www.ncbi.nlm.nih.gov/pubmed/25562937> (Accessed 7 March 2016), 2014.

31 Stammes, P., Sneep, M., de Haan, J. F., Veefkind, J. P., Wang, P. and Levelt, P. F.: Effective  
32 cloud fractions from the Ozone Monitoring Instrument: Theoretical framework and validation, J.  
33 Geophys. Res. Atmos., 113(16), 1–12, doi:10.1029/2007JD008820, 2008.

34 Stavrakou, T., Müller, J.-F., Boersma, K. F., De Smedt, I. and van der A, R. J.: Assessing the  
35 distribution and growth rates of NO<sub>x</sub> emission sources by inverting a 10-year record of NO<sub>2</sub>  
36 satellite columns, Geophys. Res. Lett., 35(10), L10801, doi:10.1029/2008GL03521, 2008.

37 Streets, D. G., Canty, T., Carmichael, G. R., de Foy, B., Dickerson, R. R., Duncan, B. N.,  
38 Edwards, D. P., Haynes, J. A., Henze, D. K., Houyoux, M. R., Jacob, D. J., Krotkov, N. A.,  
39 Lamsal, L. N., Liu, Y., Lu, Z., Martin, R. V., Pfister, G. G., Pinder, R. W., Salawitch, R. J. and  
40 Wecht, K. J.: Emissions estimation from satellite retrievals: A review of current capability,  
41 Atmos. Environ., 77, 1011–1042, doi:10.1016/j.atmosenv.2013.05.051, 2013.

42 Theys, N., De Smedt, I., van Gent, J., Danckaert, T., Wang, T., Hendrick, F., Stavrakou, T.,

1 Bauduin, S., Clarisse, L., Li, C., Krotkov, N., Yu, H., Brenot, H. and Van Roozendael, M.:  
2 Sulfur dioxide vertical column DOAS retrievals from the Ozone Monitoring Instrument: Global  
3 observations and comparison to ground-based and satellite data, *J. Geophys. Res. Atmos.*,  
4 120(6), 2470–2491, doi:10.1002/2014JD022657, 2015.

5 Tian, H., Qiu, P., Cheng, K., Gao, J., Lu, L., Liu, K. and Liu, X.: Current status and future trends  
6 of SO<sub>2</sub> and NO<sub>x</sub> pollution during the 12th FYP period in Guiyang city of China, *Atmos.*  
7 *Environ.*, 69, 273–280, doi:10.1016/j.atmosenv.2012.12.033, 2013.

8 Tong, D. Q., Lamsal, L., Pan, L., Ding, C., Kim, H., Lee, P., Chai, T., Pickering, K. E. and  
9 Stajner, I.: Long-term NO<sub>x</sub> trends over large cities in the United States during the great  
10 recession: Comparison of satellite retrievals, ground observations, and emission inventories,  
11 *Atmos. Environ.*, 107, 70–84, doi:10.1016/j.atmosenv.2015.01.035, 2015.

12 Twohy, C. H.: Nitrogenated organic aerosols as cloud condensation nuclei, *Geophys. Res. Lett.*,  
13 32(19), L19805, doi:10.1029/2005GL023605, 2005.

14 US Department of Veterans Affairs: Sulfur Fire at Mishraq State Sulfur Mine - Public Health,  
15 [online] Available from: <http://www.publichealth.va.gov/exposures/mishraq-sulfur-fire/index.asp>  
16 (Accessed 7 March 2016), 2015.

17 US EIA: Coal plants without scrubbers account for a majority of U.S. SO<sub>2</sub> emissions - Today in  
18 Energy - U.S. Energy Information Administration (EIA), [online] Available from:  
19 <http://www.eia.gov/todayinenergy/detail.cfm?id=4410> (Accessed 7 March 2016), 2010.

20 US EPA: National Emissions Inventory (NEI) Air Pollutant Emissions Trends Data, [online]  
21 Available from: <http://www.epa.gov/air-emissions-inventories/national-emissions-inventory>  
22 (Accessed 7 March 2016), 2015.

23 US EPA: Criteria Air Pollutants, [online] Available from: [https://www.epa.gov/criteria-air-](https://www.epa.gov/criteria-air-pollutants)  
24 [pollutants](https://www.epa.gov/criteria-air-pollutants) (Accessed 7 March 2016), 2016.

25 Valin, L. C., Russell, A. R. and Cohen, R. C.: Variations of OH radical in an urban plume  
26 inferred from NO<sub>2</sub> column measurements, *Geophys. Res. Lett.*, 40(9), 1856–1860,  
27 doi:10.1002/grl.50267, 2013.

28 Valks, P., Pinardi, G., Richter, A., Lambert, J. C., Hao, N., Loyola, D., Van Roozendael, M. and  
29 Emmadi, S.: Operational total and tropospheric NO<sub>2</sub> column retrieval for GOME-2, *Atmos.*  
30 *Meas. Tech.*, 4(7), 1491–1514, doi:10.5194/amt-4-1491-2011, 2011.

31 van der A, R. J., Peters, D. H. M. U., Eskes, H., Boersma, K. F., Van Roozendael, M., De Smedt,  
32 I. and Kelder, H. M.: Detection of the trend and seasonal variation in tropospheric NO<sub>2</sub> over  
33 China, *J. Geophys. Res. Atmos.*, 111(12), 1–10, doi:10.1029/2005JD006594, 2006.

34 van der A, R. J., Eskes, H. J., Boersma, K. F., van Noije, T. P. C., Van Roozendael, M., De  
35 Smedt, I., Peters, D. H. M. U. and Meijer, E. W.: Trends, seasonal variability and dominant NO<sub>x</sub>  
36 source derived from a ten year record of NO<sub>2</sub> measured from space, *J. Geophys. Res.*, 113(D4),  
37 D04302, doi:10.1029/2007JD009021, 2008.

38 Vautard, R., Cattiaux, J., Yiou, P., Thépaut, J.-N. and Ciais, P.: Northern Hemisphere  
39 atmospheric stilling partly attributed to an increase in surface roughness, *Nat. Geosci.*, 3(11),  
40 756–761, doi:10.1038/ngeo979, 2010.

41 Veefkind, J. P., Aben, I., McMullan, K., Förster, H., de Vries, J., Otter, G., Claas, J., Eskes, H. J.,  
42 de Haan, J. F., Kleipool, Q., van Weele, M., Hasekamp, O., Hoogeveen, R., Landgraf, J., Snel,



1 R., Tol, P., Ingmann, P., Voors, R., Kruizinga, B., Vink, R., Visser, H. and Levelt, P. F.:  
2 TROPOMI on the ESA Sentinel-5 Precursor: A GMES mission for global observations of the  
3 atmospheric composition for climate, air quality and ozone layer applications, *Remote Sens.*  
4 *Environ.*, 120, 70–83, doi:10.1016/j.rse.2011.09.027, 2012.

5 Vestreng, V., Ntziachristos, L., Semb, a., Reis, S., Isaksen, I. S. a. and Tarrason, L.: Evolution  
6 of NO<sub>x</sub> emissions in Europe with focus on road transport control measures, , (x), 1503–1520,  
7 doi:10.5194/acp-9-1503-2009, 2009.

8 Vinken, G. C. M., Boersma, K. F., van Donkelaar, A. and Zhang, L.: Constraints on ship NO<sub>x</sub>  
9 emissions in Europe using GEOS-Chem and OMI satellite NO<sub>2</sub> observations, *Atmos. Chem.*  
10 *Phys.*, 14(3), 1353–1369, doi:10.5194/acp-14-1353-2014, 2014a.

11 Vinken, G. C. M., Boersma, K. F., Maasakkers, J. D., Adon, M. and Martin, R. V.: Worldwide  
12 biogenic soil NO<sub>x</sub> emissions inferred from OMI NO<sub>2</sub> observations, *Atmos. Chem. Phys.*, 14(18),  
13 10363–10381, doi:10.5194/acp-14-10363-2014, 2014b.

14 Witte, J. C., Schoeberl, M. R., Douglass, A. R., Gleason, J. F., Krotkov, N. A., Gille, J. C.,  
15 Pickering, K. E. and Livesey, N.: Satellite observations of changes in air quality during the 2008  
16 Beijing Olympics and Paralympics, *Geophys. Res. Lett.*, 36(17), L17803,  
17 doi:10.1029/2009GL039236, 2009.

18 Zhang, Q., Streets, D. G., He, K., Wang, Y., Richter, A., Burrows, J. P., Uno, I., Jang, C. J.,  
19 Chen, D., Yao, Z. and Lei, Y.: NO<sub>x</sub> emission trends for China, 1995 - 2004: The view from the  
20 ground and the view from space, *J. Geophys. Res. Atmos.*, 112(22), doi:10.1029/2007JD008684,  
21 2007.

22 Zhang, Q., Streets, D. G. and He, K.: Satellite observations of recent power plant construction in  
23 Inner Mongolia, China, *Geophys. Res. Lett.*, 36(15), doi:10.1029/2009GL038984, 2009.

24 Zhang, X.-P. and Cheng, X.-M.: Energy consumption, carbon emissions, and economic growth  
25 in China, *Ecol. Econ.*, 68(10), 2706–2712, doi:10.1016/j.ecolecon.2009.05.011, 2009.

26 Zhao, B., Wang, S., Wang, J., Fu, J. S., Liu, T., Xu, J., Fu, X. and Hao, J.: Impact of national  
27 NO<sub>x</sub> and SO<sub>2</sub> control policies on particulate matter pollution in China, *Atmos. Environ.*, 77,  
28 453–463, doi:10.1016/j.atmosenv.2013.05.012, 2013.

29 Zhou, Y., Brunner, D., Boersma, K. F., Dirksen, R. and Wang, P.: An improved tropospheric  
30 NO<sub>2</sub> retrieval for OMI observations in the vicinity of mountainous terrain, *Atmos. Meas. Tech.*,  
31 2(2), 401–416, doi:10.5194/amt-2-401-2009, 2009.

32 Zhou, Y., Brunner, D., Hueglin, C., Henne, S. and Staehelin, J.: Changes in OMI tropospheric  
33 NO<sub>2</sub> columns over Europe from 2004 to 2009 and the influence of meteorological variability,  
34 *Atmos. Environ.*, 46, 482–495, doi:10.1016/j.atmosenv.2011.09.024, 2012.

35 Zyrichidou, I., Koukouli, M. E., Balis, D. S., Katragkou, E., Poupkou, A., Kioutsoukis, I.,  
36 Markakis, K., Melas, D., Van Der A, R., Boersma, F. K. and Van Roozendaal, M.: Comparison  
37 of satellite NO<sub>2</sub> observations with high resolution model simulations over the Balkan Peninsula,  
38 in AIP Conference Proceedings, vol. 1203, 632–637, 2010.

39 Zyrichidou, I., Koukouli, M. E., Balis, D. S., Kioutsoukis, I., Poupkou, A., Katragkou, E.,  
40 Melas, D., Boersma, K. F. and van Roozendaal, M.: Evaluation of high resolution simulated and  
41 OMI retrieved tropospheric NO<sub>2</sub> column densities over Southeastern Europe, *Atmos. Res.*, 122,  
42 55–66, doi:10.1016/j.atmosres.2012.10.028, 2013.

1

2

3

4 **Table A1 Filtering transient volcanic clouds**

Region	Threshold (DU)	Days excluded (2005-2014)
Eastern US	5	97
Eastern Europe	8	72
Eastern China	10	71
India	8	58
Middle East	8	10

5



1

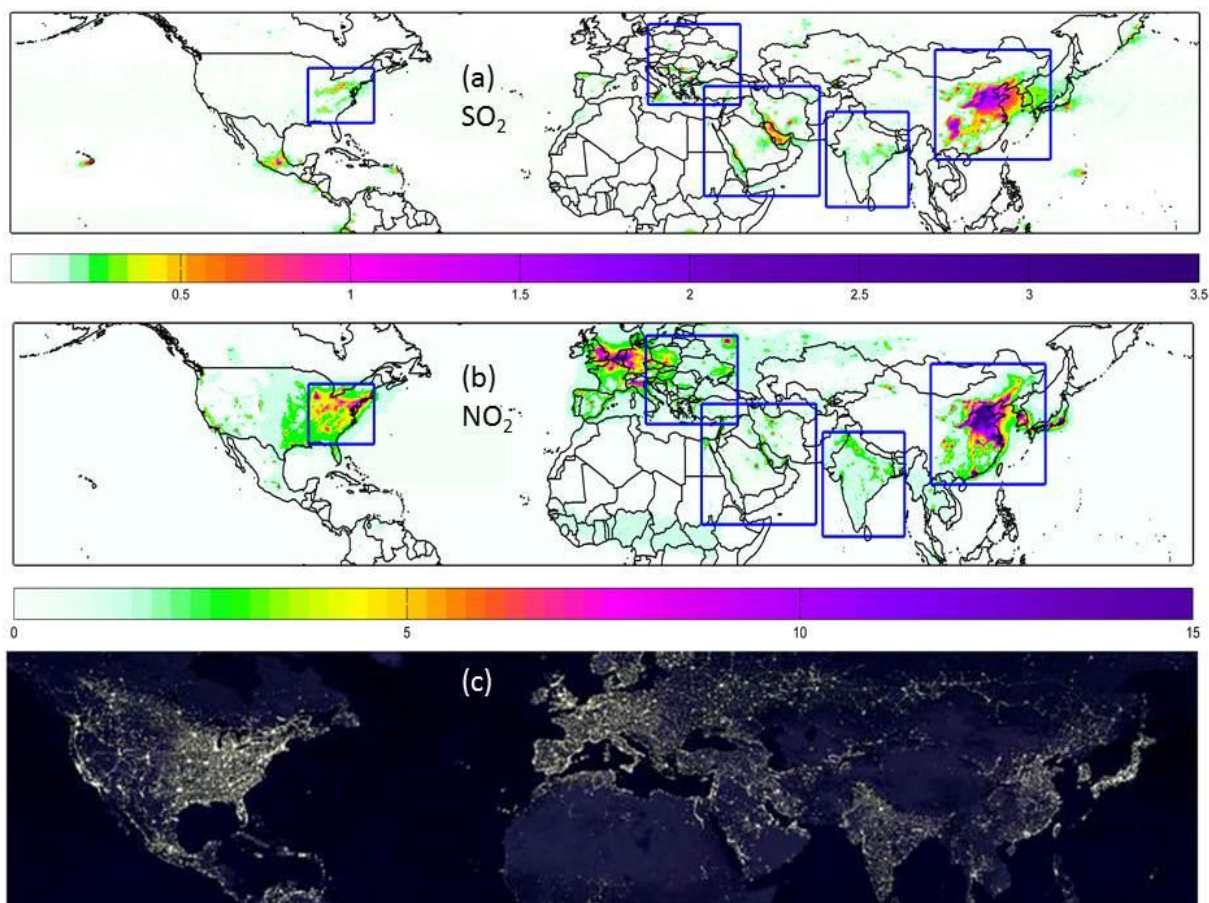


Figure 1. OMI-derived maps of PBL  $\text{SO}_2$  in Dobson Units [DU] (a) and tropospheric  $\text{NO}_2$  columns in [ $10^{15}$  molecules/cm<sup>2</sup>] (b) for 2005-2007 show enhanced pollution levels around major cities and industrial centers, seen also in the “Earth at Night” (city lights) map (c), courtesy of Aura EPO team.

2

3

4

5

1

2 F2

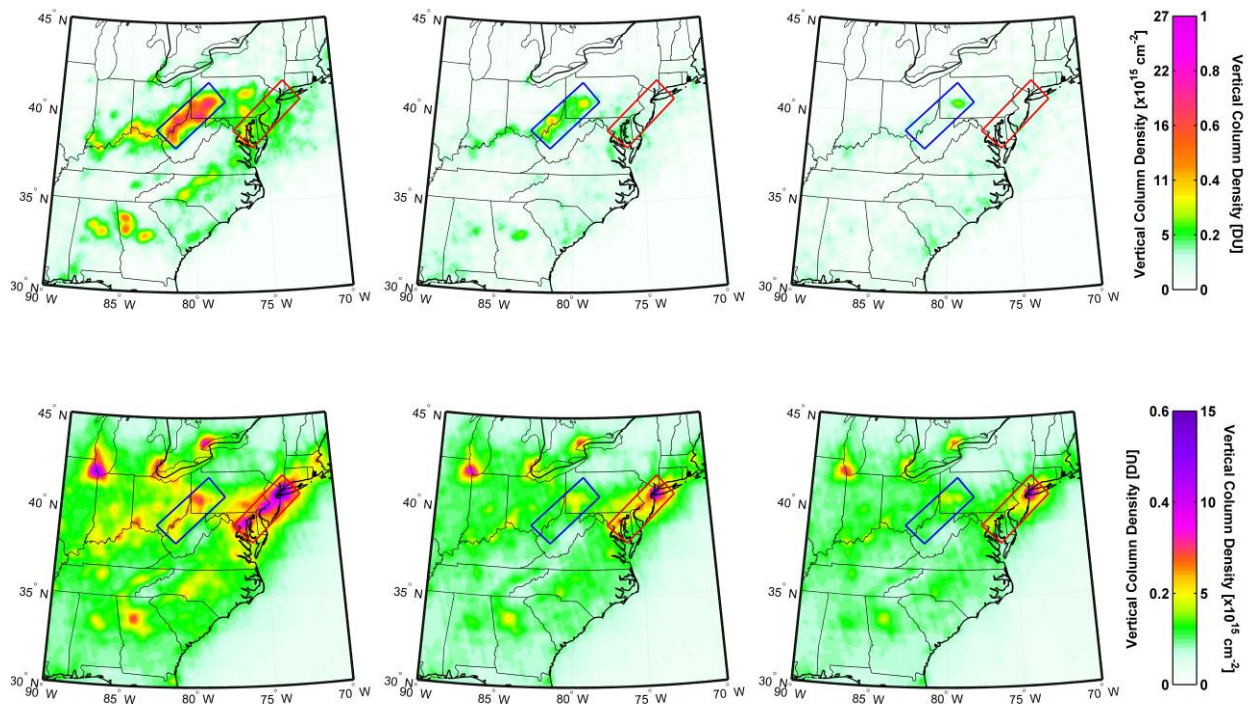


Figure 2. 3-year average OMI SO<sub>2</sub> (top) and tropospheric NO<sub>2</sub> (bottom) regional maps over eastern US for 3 periods: 2005-2007 (left), 2009-2011 (middle) and 2013-2015 (right). Blue box outlines Ohio River Valley and SW Pennsylvania (ORV) region with largest SO<sub>2</sub> emissions from coal-fired power plants. Red box outlines megalopolis from Washington, DC to New York along the I-95 interstate highway (I-95 corridor) with largest NO<sub>2</sub> from mobile sources.

3

4

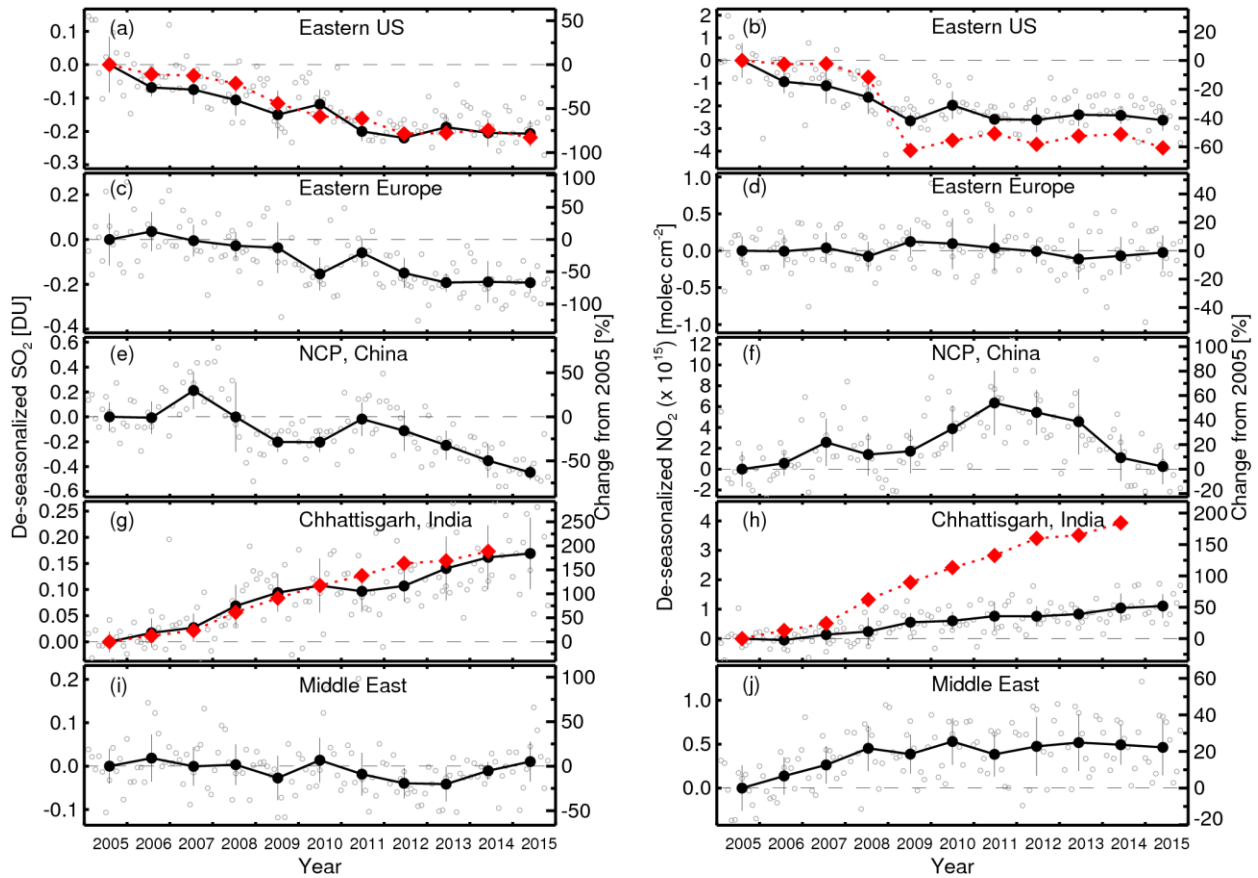


Figure 3. Relative changes (compared to 2005) in OMI PBL  $\text{SO}_2$  columns (left) and tropospheric  $\text{NO}_2$  columns (right) over 5 world's most polluted regions: (a) and (b): Ohio River Valley and southwestern Pennsylvania (ORV) in eastern US (ORV - blue box in Fig. 2); (c) and (d): Maritsa Iztok Power Plants in Bulgaria (blue box in Fig. 4); (e) and (f): North China Plain (NCP - blue box in Fig.5); (g) and (h): NE India (blue box in Fig. 6); (i) and (j): Persian Gulf (blue box in Fig. 7). Gray circles show de-seasonalized monthly columns (see details in Appendix B). Black filled circles show annual means. Vertical bars show standard deviations. Red diamonds show bottom-up emission estimates for power plants in ORV and from coal-fired power plants in NE India (Chhattisgarh and Odisha region – blue box in Fig. 4).

1

2

3

1

2 F4

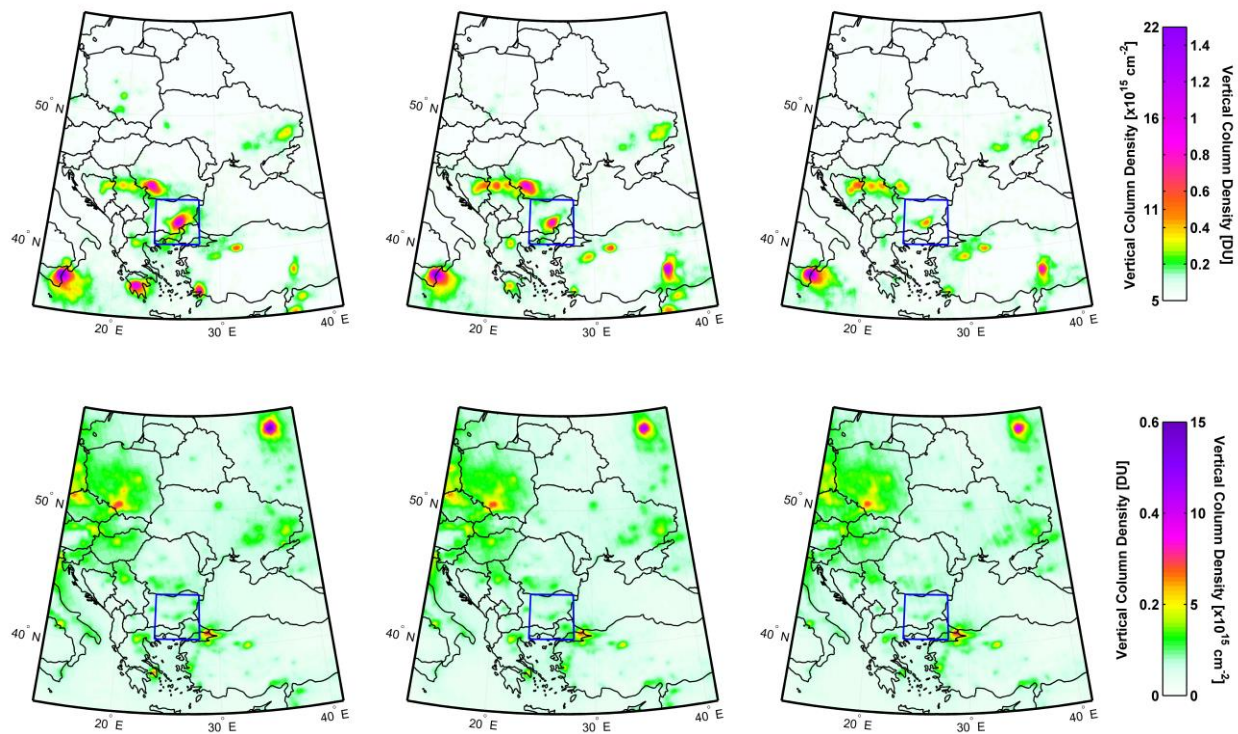


Figure 4: Same as Fig. 2, but for Eastern Europe. The largest  $\text{SO}_2$  source in the domain is the Etna volcano in Sicily, Italy. The blue box is centered on  $\text{SO}_2$  polluted area around Maritsa Iztok coal mining region and the largest coal-fired power plants in southeastern Bulgaria.

3

4

5

6

7

8



1

2

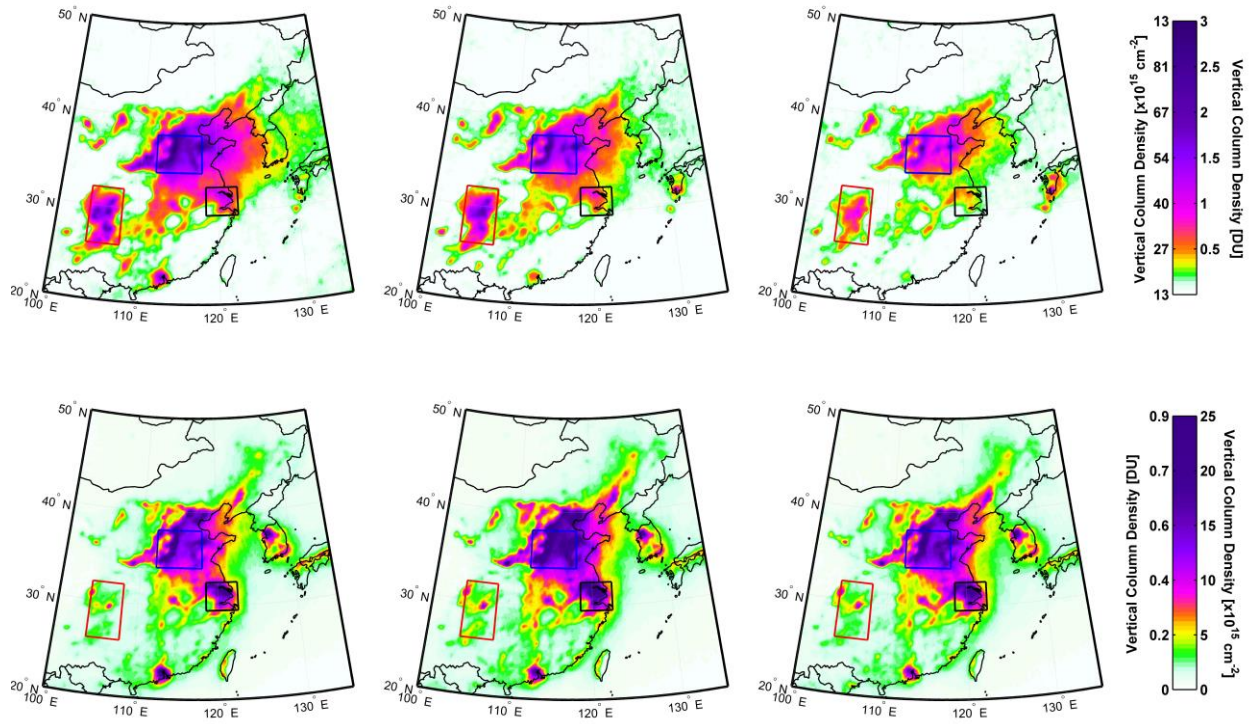


Figure 5. Similar to Figure 2 but for Eastern China. Blue box outlines North China Plane (NCP) also represented in Fig.3, red box - Sichuan Basin (SB) and black box represent Yangtze River Delta (YRD). The boxes are also shown in Fig. S1, S3 and S4.

3

4

5

6 F6

7

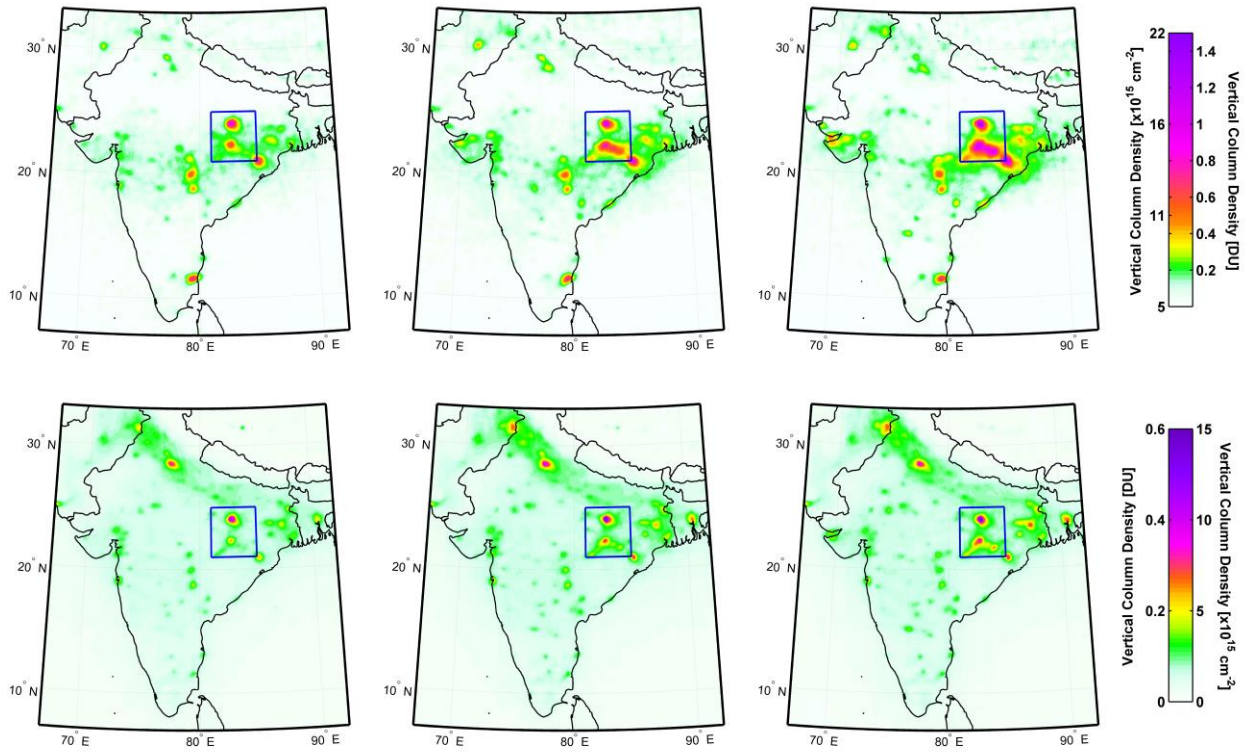


Figure 6. Similar to Fig. 2 but for India. Blue box outlines industrial regions in Chhattisgarh and Odisha, one of India's most active areas in terms of building new coal-fired power plants. The region is shown in Fig.3.

1

2

3

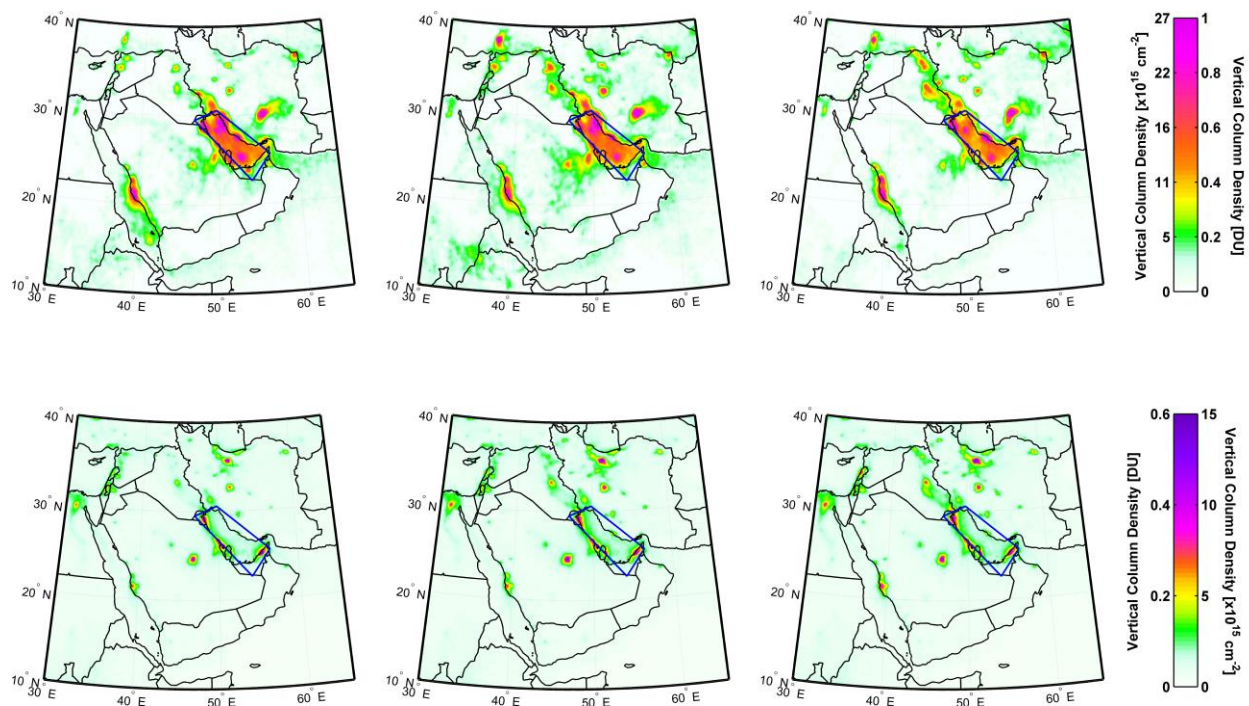


Figure 7. Similar to Fig. 2 but for the Middle East. Blue box outlines Persian Gulf region with high  $\text{SO}_2$  and  $\text{NO}_2$  levels due to oil and gas operations.

1

2

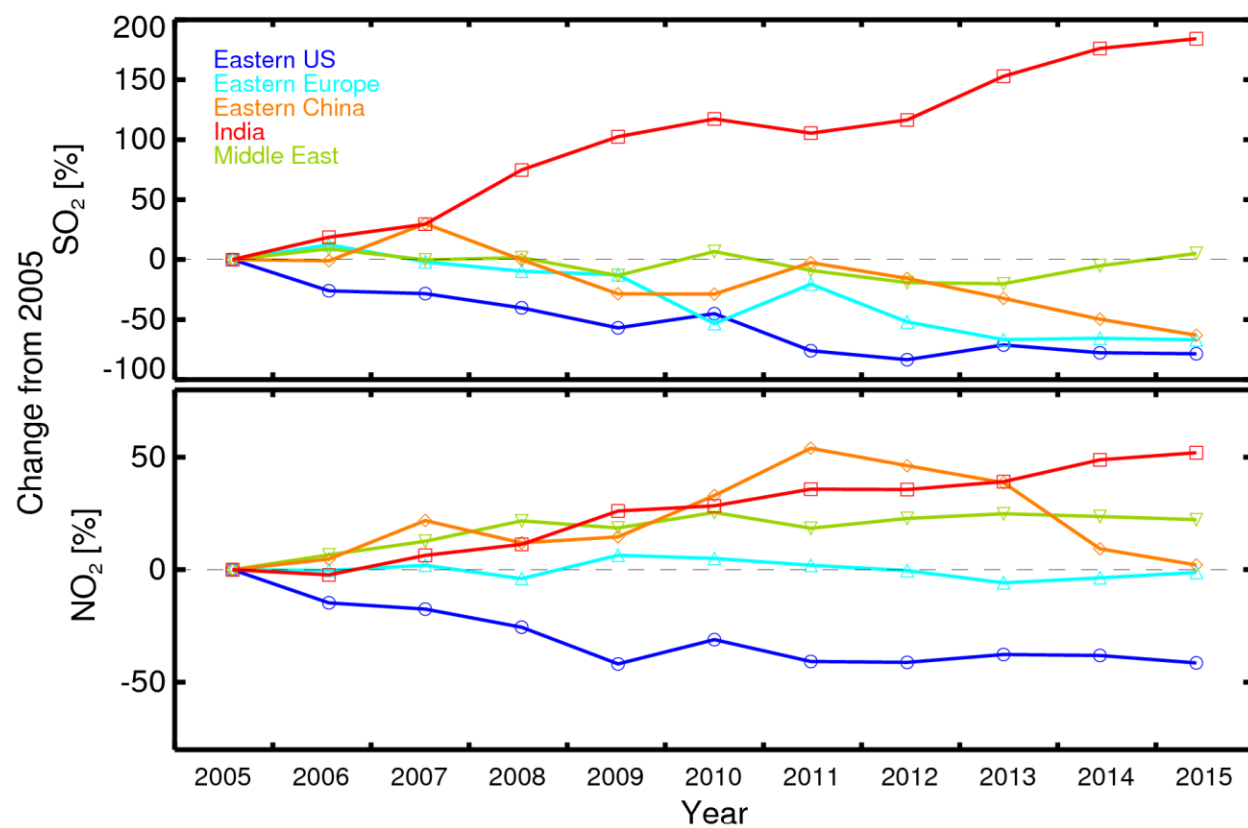


Figure 8. Percent change in OMI annual average columns since 2005: SO<sub>2</sub> (top) and NO<sub>2</sub> (bottom) over the world's most polluted regions discussed in this study.